Sustainable Aviation Fuel from Syngas through Higher Alcohols

Mäki-Arvela, Päivi; Aho, Atte; Simakova, Irina; Yu. Murzin, Dmitry

Published in:
ChemCatChem

DOI:
10.1002/cctc.202201005

E-pub ahead of print: 28/09/2022

Document Version
Final published version

Document License
CC BY

ChemCatChem

Review
doi.org/10.1002/cctc.202201005

Chemistry Europe
European Chemical Societies Publishing

www.chemcatchem.org

Sustainable Aviation Fuel from Syngas through Higher Alcohols

Päivi Mäki-Arvela,[a] Atte Aho,[a] Irina Simakova,[b] and Dmitry Yu. Murzin*[a]

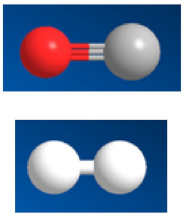

K-CuFe-CNF
K-CuFe/MFI (hierarchical)
Cu_xCo_y
275-325°C, 1 - 5 MPa
$Co_xMo@C$
Na-CoFe
K-CoRhMo

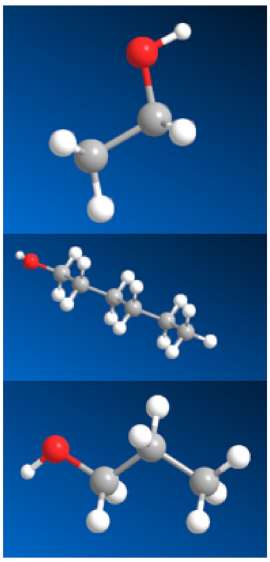

- Alkali suppresses hydrogenation
- Interfacial contact between metals
- Formation of active carbide species: Co_2C, Fe_5C_2, Cu-Fe_2C_2

The current review critically summarizes recent developments in transformations of syngas to higher alcohols. Although higher alcohols have found applications as fuel additives, detergents and plastics for a long while, transformation of alcohols to jet fuel has attained recent interest due to an urgent need to develop jet fuels from sustainable sources. Fermentation of lignocellulosic-based sugars to ethanol as a technology does not compete with the food chain supply being thus a potentially acceptable route if economically viable. An alternative method is to gasify biomass to produce syngas, which can further be transformed to higher alcohols through several pathways. Jet fuel range alkanes are obtained from alcohols via oligomerisation, dehydration and hydrogenation. The highest space time yields of higher alcohols of 0.61 g/(g_{cat}h) is obtained over a bimetallic copper-iron catalyst supported on a hierarchical zeolite at 300 °C and 5 MPa. Furthermore, copper-cobalt and cobalt-manganese compositions are promising for the direct synthesis of higher alcohols from syngas, where one of the challenges is to suppress formation of alkanes and CO_2 and increase selectivity to higher alcohols. From the mechanistic point of view, it has been proposed to use dual-site catalysts, where one site promotes hydrogenation, while the other site is required for the chain growth. In addition to selection of the optimum reaction conditions and catalyst properties, kinetic modelling, thermodynamics and scale up issues are discussed.

1. Introduction

An extensive research is currently performed to transform biomass derived feedstock to fuels and chemicals. Syngas, produced by gasification of biomass[1] is a potential renewable feedstock, which would promote sustainable development of chemical industry. It was also pointed out in[2] that when syngas is derived from coal or biomass, the H_2/CO ratio is low which is beneficial for formation of higher alcohols, typically defined as alcohols with a carbon number equal or higher than two.[2] Such higher alcohols are important compounds to be used as fuel additives directly or as feedstock for production of detergents, plastics and lubricants.[3] Higher alcohols as fuel additives increase octane rating of gasoline[4,5] being overall beneficial because of their lower volatility and better solubility in comparison to methanol. In addition, soot and nitrogen oxide formation can be reduced by addition of higher alcohols to gasoline.[1]

Industrial application of direct syngas transformation to higher alcohols is, however, challenging[6] and limited due to low selectivity.

It has recently been emphasized that there is an increasing demand of jet fuel, which would double the jet fuel consumption and increase CO_2 emissions six times by 2050.[7] A need to produce sustainable aviation fuel (SAF) has been widely addressed recently.[10] Some efforts towards climate friendly direction have already been made, e.g. the European Commission has established objectives for jet fuel production[7] and sustainable aviation fuels (SAF) comprised of liquid drop-in fuels produced from renewable sources have been identified to have a high potential to reduce GHG emissions of conventional jet fuels.[8,9] At the current level of aviation industry and types of airplanes in operation, there is hardly any alternative to liquid jet fuels, which should be of high energy content and density. Apparently, when jet fuels are produced from biomass derived sources, their CO_2 emissions decrease.[11] One emerging method to produce jet fuels from bio-derived alcohols is to convert alcohols by their dehydration to olefins followed by oligomerization and hydrogenation giving alkanes,[10,12] which represent ca. 20% of jet fuel. The conventional method to produce bioalcohol is fermentation of e.g. sugarcane as practiced in Brazil, which is unfortunately competing with the food supply chain. Production of ethanol from lignocellulosic feedstock via hydrolysis and fermentation is demanding[13,14] resulting in a large number of by-products. Because in syngas transformation to higher alcohols typically ethanol is the main component, this could also promote such process as a step in for jet fuel alkane production. Bioethanol can in turn be catalytically transformed to biobutanol.[15] In addition to alkanes, current jet fuels contain cycloalkanes ca. 27%, which could be obtained from lignin.[16] According to jet fuel specifications, the fraction of isoalkanes and aromatics is ca. 33% and 20%, respectively. The former ones are produced via hydroisomerization of alkanes over acidic catalysts,[17] while butanol can be transformed to aromatics over H-ZSM-5 catalyst[18] and its isomer isobutanol over Ga–H-ZSM-5 catalyst.[18] In addition, butene is formed catalytically from ethanol over Zn–Y/Beta catalyst.[19] and over Ag-ZrO_2/SiO_2 catalyst.[20] Furthermore, jet fuels were synthesized from ethylene and ethanol containing feedstock.[21] In addition to biomass, also waste can be transformed to syngas already at commercial scale.[22] The above-mentioned routes demonstrate clearly that catalytic technologies can be applied conceptually for production of all fractions in jet fuels from biomass derived feedstock without competing with the food supply chain.

Transformation of syngas to higher alcohols is currently under intensive research[2,4,5,23–57] and several reviews have been published rather recently covering the nature of active centers „[1,54] and more specifically performance of Fe/Co catalysts and Co carbide nanocatalysts.[59] A simplified reaction scheme for syngas transformation over a bifunctional catalyst is shown in Figure 1.[40] For example copper in Cu–CFe catalyst has a higher

[a] Prof. P. Mäki-Arvela, Dr. A. Aho, Prof. D. Yu. Murzin
Johan Gadolin Process Chemistry Centre
Laboratory of Industrial Chemistry and Reaction Engineering
Åbo Akademi University
Turku/Åbo (Finland) Henriksgatan 2, 20500
E-mail: dmurzin@abo.fi
Homepage: http://users.abo.fi/dmurzin/
[b] Dr. I. Simakova
Boreskov Institute of Catalysis
Novosibirsk (Russia)

hydrogenation ability in comparison to iron thus promoting hydrogenation of aldehydes to alcohols, while iron is a key catalyst for the chain growth.[39] In addition to linear and branched alcohols also methanol, olefins and paraffins are formed. Water generated by methanol dehydration reacts via the water-gas shift reaction:

$$CO + H_2O = CO_2 + H_2 \quad (1)$$

forming undesired CO_2.

In this work the recent developments in syngas transformations to higher alcohols mainly after 2018 are summarized, especially focusing on reporting the highest space-time yields of higher alcohols with different catalysts. The reaction mechanism, thermodynamics, influence of reaction conditions, reaction kinetics and kinetic modelling are emphasized. The main parameters in addition to the catalyst selection are the H_2/CO ratio, weight hourly space velocity, temperature and pressure. From the industrial perspective, the catalyst stability is of interest as well as reaction and reactor engineering aspects, which will be also covered here.

2. Reaction Network

In syngas transformations to higher alcohols also hydrocarbons, aldehydes, CO_2 and water are formed. The main side reaction could be direct formation of methanol by CO hydrogenation. From the mechanistic viewpoint CO can, however, adsorb either dissociatively or non-dissociatively on different types of active

Associate professor Päivi Mäki-Arvela received her Doctor of Technology (chemical engineering) in 1994 at Åbo Akademi University, Turku, Finland. Her research areas are catalytic three-phase reactions, especially transformations of renewable raw materials to valuable products using heterogeneous catalysts. She has published more than 350 peer-reviewed publications, several review papers, and patents. Her research has been acknowledged by several prizes. She has served as President of the Nordic Catalysis Society and the Finnish Catalysis Society and as a board member in the European Federation of Catalysis Societies.

Dr. Atte Aho, received his Doctor of Technology (chemical engineering) in 2009 at Åbo Akademi University, Finland. His research topics are catalytic transformation of renewable feedstock and physico-chemical characterization of heterogeneous catalysts. He has published more than 100 peer reviewed journal articles.

Dr. Irina Simakova, Leading Scientist of Boreskov Institute of Catalysis (Novosibirsk, Russia) studied chemistry at Novosibirsk State University graduating in 1986 with MSc in Chemistry. In 1999 she defended her PhD thesis in Kinetics and Catalysis working at Boreskov Institute of Catalysis and was appointed in 2004 as a Head of a research group of Catalysts on Carbon Supports. In 2010 she obtained Doctor of Science degree in Chemistry from Åbo Akademi University, Turku, Finland as well as the academic title Docent (Associate Professor) from Boreskov Institute of Catalysis. She is a co-author of more than 150 peer-reviewed papers, several reviews, and 13 patents. She has supervised five PhD students and seven MSc students. The focus of her scientific interests is on developing heterogeneous nanocatalysts for various catalytic processes especially synthesis of fine organic chemicals and valorization of biomass, as well as on investigating kinetics and mechanisms of heterogeneously catalysed processes.

Professor Dmitry Yu. Murzin studied chemical engineering at the Mendeleev University of Chemical Technology in Moscow, Russia (1980–1986) and graduated with honors. He obtained his PhD (advisor Prof. M.I. Temkin) and DrSc degrees at Karpov Institute of Physical Chemistry, Moscow in 1989 and 1999, respectively. He worked at Universite Louis Pasteur, Strasbourg, France and Åbo Akademi University, Turku, Finland as a post-doc. In 1995–2000 he was associated with BASF, being involved in research, technical marketing and management. Since 2000 Prof. Murzin holds the Chair of Chemical Technology at Åbo Akademi University. He is an elected member of Academia Europaea, the Finnish Academy of Science and Letters, and holds honorary professorships from Tianjin University and St. Petersburg State Technological Institute. Prof. Murzin is an author or co-author of ca. 850 journal articles and book chapters, and several textbooks.

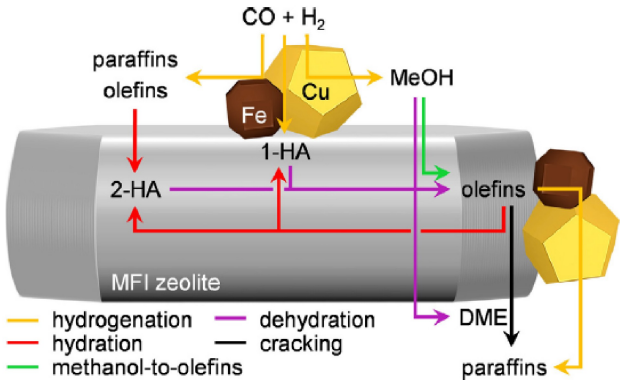

Figure 1. A simplified reaction scheme for syngas transformation to different products over K-modified Cu–CFe supported on MFI zeolite. Notation: 1-HA linear higher alcohols, 2-HA branched higher alcohols, DME dimethyl ether. Reproduced from ref. [40] Copyright (2019) with permission from Elsevier Ltd.

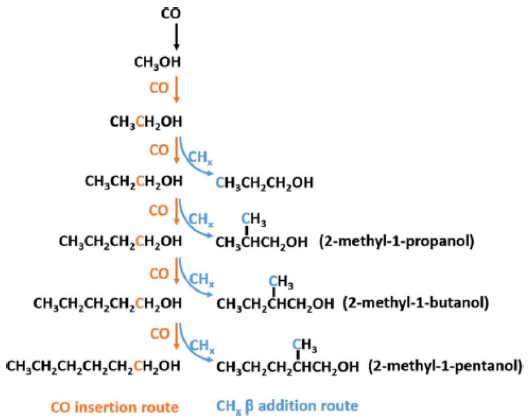

Figure 3. Formation of linear and branched alcohols by CO insertion method and CH_x β-addition, respectively. Reproduced from ref. [5] Copyright (2019) with permission from Elsevier Ltd.

sites. A dual site model developed in[60] assumes two types of sites responsible for dissociative and non-dissociative adsorption of CO, respectively. When CO is adsorbed non-dissociatively, it can be inserted into methanol as follows:

$$^{13}CH_3OH + {}^{12}CO/H_2 \; {}^{13}CH_3{}^{12}CH_2OH \quad (2)$$

This insertion mechanism of CO into methanol has been confirmed by ^{13}C NMR studies over Cs–Cu/ZnO catalyst already several decades ago.[61] Several dual site catalysts have been reported in the literature including Rh–CoMn and Ru–CoMn.[44] The same authors[48] also emphasized that the C_2Hx* adsorbed species are necessary for formation of C3 oxygenation products. Recently the mechanism for higher alcohol formation over CuZnAl–CoMo catalyst was investigated using in situ DRIFTs-MS technique together with CD_3OD in a carrier gas H_2/CO with the ratio of 2, while heating the reactor from 50 °C to 250 °C and then keeping the temperature at 250 °C.[48] It was demonstrated that CH_xO* is formed over CuZn sites migrating thereafter to CoMn sites, where CHx* are adsorbed. Finally, these two species react with each other forming CH_3HDO as depicted in Figure 2.

Besides linear higher alcohols also secondary alcohols are formed with syngas as the feedstock.[2,28,41] A schematic picture of their formation is depicted in Figure 3.[5] As follows from Figure 3 linear alcohols are generated through the CO insertion route, while for the branched ones β-addition of CH_x species is

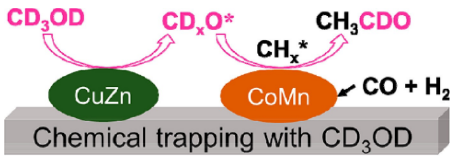

Figure 2. Proposed reaction mechanism for formation of alkanal based on in situ DRITS-MS results. Reproduced from ref. [49] Copyright (2021) with permission from ACS publications.

required. Among the formed oxygenates small amounts of aldehydes are also present.

Typically, similar yields of hydrocarbons and alcohols are obtained reflecting close chain growth probability of hydrocarbons and alcohols. The active sites in Co and Fe containing materials are carbides, such as Co_2C[29] and e'-$(Co_xFe_{1-x})_{2.2}C$[52] which are formed during catalysis upon exposure to the synthesis gas. The primary product according to the carbide mechanism for the higher alcohol formation is an olefin which is rapidly hydrogenated to the corresponding alkane. One important parameter, related to higher alcohols formation from syngas is the chain growth probability, α, which is essential for calculations of the weight fraction of alcohols, W_n,[4,5,28,29–31,33,34–37,42,44,48,52]

$$W_n/n = (1\text{-}\alpha^2)/\alpha^*\alpha^n \quad (3)$$

where W_n is just as a function of the carbon number n and the parameter α denotes chain growth. After linearization this equation can be written as:

$$ln\left(\frac{W_{ni}}{n}\right) = nln\alpha + ln\left(\frac{(1-\alpha)^2}{\alpha}\right) \quad (4)$$

giving a possibility to calculate α-values for formation of alcohols and hydrocarbons for different catalysts by plotting $\ln(W_{ni}/n)$ vs *n*.

Analogously α can be calculated based on the molar fractions as:

$$ln\left(\frac{c_{ni}}{n}\right) = nln\alpha + ln\left(\frac{(1-\alpha)^2}{\alpha}\right) \quad (5)$$

in which c_{ni} is the molar fraction of the product. Alternatively the following equation can be used[5] to describe selectivity to a product *i*, S_{ni}:

$$\left(\frac{S_{ni}}{n}\right) = \alpha^{n-1}(1-\alpha) \quad (6)$$

Water is also generated during dehydration of an alcohol facilitating CO_2 formation by the water gas shift reaction [eq. (1)]. In some cases, no CO_2 formation[28] or low CO_2 selectivity[2,28,29,36,38,46,47,54] have been reported. Due to the parallel nature for hydrocarbons and alcohols formation resulting in higher amounts of CO_2 at higher conversion levels, typically a compromise between conversion and selectivity is required which should be taken into account when establishing economic feasibility of the process.[32] Due to the consecutive reaction network, typically higher selectivities to hydrocarbons, and CO_2 are reported, whereas fractions of methanol, higher alcohols and olefin are decreasing when increasing conversion.[32]

The undesired methane can be either formed by dehydration and hydrogenation of methanol as well as from CO and H_2 through methanation:

$$CO + 3H_2 = CH_4 + H_2O \quad (7)$$

The latter reaction is very exothermic, with $\Delta H = -206.28$ kJ/mol.[62] In addition, polymerization and termination reactions occur in the chain via β-hydrogen elimination and hydrogenation, respectively.[33]

3. Catalyst Selection

The recent results from syngas transformation to higher alcohols are given in Table 1 while the catalyst properties are shortly summarized in Table 2. Several types of catalysts have been recently tested in this reaction including bimetallic Cu–CFe (Table 1, entries 1–4),[1,35,49,54] Cu–Co (Table 1, entries 6–15),[2,34,38,45,46] Co–Fe (Table 1, entry 16),[52] Co–Rh (Table 1, entry 17),[44] Co catalyst (Table 1, entry 18),[28] MoS_2 (Table 1, entries 21, 22, 23),[4,58] and some mono- and multimetallic catalysts. As mentioned above both chain growth and hydrogenation ability are required for synthesis of higher alcohols. Among the studied catalyst several metals have hydrogenation ability, i.e. Cu, Co, Au, Rh, Mo_2S, while the chain growth behaviour is attributed to Fe, Co and Rh.[63] In addition, alkali promoters and metal oxides, MnO_x have been used to suppress hydrogenation. Furthermore, in some cases the metal function is embedded into the support material, promoting formation of higher alcohols. A delicate balance is required between these two functions, as if a metal is too active in hydrogenation, methane, hydrocarbons and lower alcohols are formed. Methanation is also an undesired reaction, which has been suppressed in several recent studies.[28,36,38] For example a catalyst exhibiting interfacial Fe_5C_2–Cu species can suppress methanation.[36] Another catalyst producing low amounts of methane is a multimetallic CuZnAlZr catalyst.[38]

The highest space-time yield for higher alcohols has been obtained with a potassium promoted Cu–CFe-catalyst which was supported on a hierarchical zeolite (Table 1, entry 4) (Figure 4) with the metal particle size of 16.8 nm (Table 2, entry 4).[39] Another promising catalyst is K–CuFe/CNF (Table 1, entry 1). For this catalyst exhibiting the Cu/Fe ratio of 2, the optimum Cu particle size was ca. 10 nm, while iron was highly dispersed with the particle size of 4.9 nm (Table 2, entry 1). Potassium, which suppresses hydrogen adsorption capacity, has also an electronic effect.

Furthermore, the higher alcohols selectivity decreased with increasing the Cu particle size above 10 nm.[41] When this result is compared with the performance of other Cu–CFe catalysts (Table 1, entry 1, 3) it is clearly visible that when the particle size of the alloy Cu_4Fe_1 was relatively large, 21 nm, CO_2 formation was elevated (Table 1, entry 3, Figure 5b).[36]

It should also be pointed out that in[37] the data were generated at 5.0 MPa and with the H_2/CO ratio of 1.5, which were considered as optimized conditions for this catalyst. This makes the direct comparison of the results obtained at different conditions challenging. In addition, K-modified Cu–CFe supported on a hierarchical MFI zeolite was a rather efficient catalyst for higher alcohol synthesis giving 44% selectivity to alcohols at 4% conversion of CO (Figure 6a).[40] Co supported on graphene oxide -mesoporous silica was also reasonable selective towards higher alcohols (Table 2, entry 13)[29] giving very low amounts of CO_2 (Figure 6b). It was proposed that graphene oxide can act as an electron donor enhancing carbides formation, which in turn enhances higher alcohol synthesis. In that case the cobalt particle size was only 8.6 nm (Table 2, entry 13).[25] Interestingly it was also confirmed that the alcohol selectivity at the same CO conversion level was directly comparative to the ratio of Co_2C/Co determined by XRD when using catalysts with different amounts of graphene oxide (GO) in Co/GO-OMS catalysts.[29] This result clearly emphasizes the

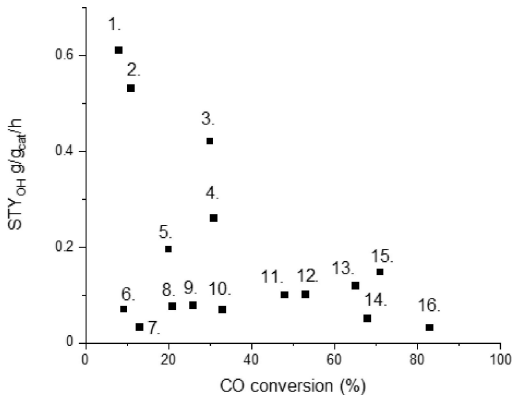

Figure 4. Space-time yield of higher alcohols in syngas transformations over different catalysts. Notation: 1. K–CuFe supported on hierarchical MFI,[40] 2. K–CuFe/CNF,[41] 3. K–CoRhMo supported on carbon nanohorn,[25] 4. CoFe-300–CNa (300 denotes to reduction temperature, °C),[52] 5. Au–CFe_3O_4,[53] 6. $CuFeMnGO_{0.3}$ (GO indicates graphene oxide)[54] 7. $CuCoAlZnOZrO_2$,[34] 8. $CoMnO_x$-quasi MOF-74 (MOF denotes metal organic framework),[28] 9. CoMn/CuZnAlZr,[38] 10. RhCoMn,[44] 11. $Co_{4.7}Mo$@C derived from polyoxymetalate,[35] 12. Cu_4Fe_1,[36] 13. CuZnO,[37] 14. CuFe supported on hierarchical hollow silica spheres (HHSS),[50] 15. $Cu_{0.25}Co_{0.75}$,[46] and 16. Co_3Cu_1KIT-6.[2] The reaction conditions and catalyst properties are given in Table 1 and 2, respectively, for each catalyst.

Table 1. The state-of-art results from production of higher alcohols (HA) from syngas over different catalysts. Notation: STY: space-time yield, S denotes selectivity, α is chain growth probability, OH alcohol, HC hydrocarbon. Notation: AC active carbon, GO graphene oxide, HHSS hierarchical hollow silica spheres, MOF metal organic framework, GO graphene oxide, OMS ordered mesoporous.

Entry	Catalyst	Reaction Conditions										Alcohol distribution [wt%]				
		T [°C]	P [MPa]	H_2/CO	GHSV [mL/g_{cat}.h]	CO conversion [%]	STY_{OH} [g/g_{cat}.h][d]	S_{CO2} [%]	S_{CH4} [%]	S_{ROH} [%]	S_{HC} [%]	MeOH	C_2+OH	αOH	αHC	Ref.
1	K–CuFe–CNF	275	5	1.5	32000	11	0.53	12	n.a.	44	46	16	84	n.a.	n.a.	[41]
2	CuFe supported on hierarchical hollow silica spheres (HHSS) CuFe@ HHSS	300	3	2.0	5000 b	65	0.118	10	n.a.	47	40	40	60	n.a.	n.a.	[50]
3	$Cu_4Fe_1Mg_4$ mixed metal oxide	260	1	2.0	2400	53	0.101	30	3.7	30	37	8.7	91	0.72[e]	0.70[e]	[36]
4	K–CuFe supported on hierarchical MFI	300	5	1	32000	8	0.61	13	n.a.	45	36	0	100	n.a.	n.a.	[40]
5	CuFeMn–GO0.3	260	3.0	2.0	3600[b]	9.3	0.070	1	n.a.	74	25	16.6[f]	83.4[f]	n.a.	n.a.	[54]
6	Cu/ZnO	300	4	2.0	6000[b]	63	0.051	55	n.a.	20	40	6	94	0.256	0.424	[37]
7	CuCoMn	270	3	2.5	7500	29.7	n.a.	0.5	16.6	46	51	30[f]	70[f]	n.a.	n.a.	[46]
8	CoCu	280	6	1.0	12000	6	n.a.	30	15	41	57.4	46	54	n.a.	n.a.	[33]
9	3Cu-5Co/(Mn–Al)	260	5	2	5000	33.4	0.063	14.1	n.a	39.7[a]	46.2[a]	42.7[f]	57.3[f]	n.a.	n.a.	[55]
10	CuCoAlZnOZrO2	250	5	2.0	4000	13	0.032	8[a]	40[a]	42[a]	40[a]	17	83	0.549[g]	0.399[g]	[34]
11	Co3Cu1KIT-6	270	3	2.0	12800	83	0.039 mol/[g_{cat}h]	0.8	30	46	53	34	64	n.a.	n.a.	[2]
12	$Cu0.25Co_{0.75}$	250	3	2.0	3900[b]	71	0.147	n.a.	n.a.	14[c]	86[c]	19	81	n.a	n..a.	[46]
13	Co-3GO-OMS	225	3	2.0	10800	35.4	0.010	0.5	22.2	48.3	43.4	43.4[f]	48.3[f]	n.a	n.a.	[2]
14	$Co_{4.7}$Mo@C	275	3	2.0	15000	48	0.123 (0.099)	21	28	12	n.a.	19.7	80.3	0.56[g]	n.a.	[35]
15	Co_1Mn/AC (AC active carbon)	220	3	2.0	2000	29.1	0.047	2.4	8.1	21.4	68.1	7.6	92.4	0.69[e]	0.72[e]	[56]
16	CoFe-300–CNa	260	3	2.0	10800	24	0.27 (0.196)	9.7	13.2	31	60	26.3	72	0.71[e]	n.a.	[52]
17	RhCoMn	220	6	1.0	2000	33	0.071 (0.066)	16	6	34	59	n.a.	n.a.	0.66[e]	0.75[e]	[44]
18	$CoMnO_x$-quasi-MOF-74	200	3	2.0	4500	21	0.058	0.8[a]	10[a]	39[a]	60[a]	8	92	0.65[e]	0.68[e]	[28]
19	CoMn/CuZnAlZr	230	6	2.0	2000	18	0.037	3[a]	5[a]	46[a]	48.5[a]	6.8	93.2	0.74[e]	0.75[e]	[38]
20	K–CoRhMo supported on carbon nanohorn	325	9.1	1.25	2.4 h	30	0.433	n.a.	n.a.	n.a.	n.a.	n.a.	n.a.	n.a	n..a.	[25]
21	K–$NiMoS_2$	340	5	1.0	760	15	n.a.	25.8	4.6	69.4	4.6	3.8	65.8	n.a.	n.a..	[4]
22	K–MoS_2	340	8.7	1.0	4500	25	n.a.	36	32	33 (oxygenates)	4.7	25.1	75	n.a.	n.a.	[5]
23	K–MoS_2–MnAl composite	360	5.0	2	5000	27	0.115	n.a.	n.a.	68.6[a]	31.4[a]	41	59	n.a.	n.a.	[56]
24	K–Rh/Mo_2C	290	1	1.0	1200	10	n.a.	n.a.	n.a.	44	46	27	49	0.36[g]	0.47[g]	[48]
25	K–MoP/mesoporous carbon	290	1	1.0	7500	5	n.a.	1.4	19	28.5	29.5	29	30	0.43[e]	0.55[e]	[47]
26	Au–Fe_3O_4	260	3	1.0	4800	20	0.195	12	5	53[a]	47[a]	26	73	n.a.	n.a.	[53]

[a] wt%, [b] h^{-1}, [c] CO_2 free, [d] in parenthesis STY for higher alcohols, [e] α by weight basis from eq. (3), [f] molar basis, [g] α by molar basis from eq. (5), [h] $m^3STP/(g_{cat}h)$.

Table 2. Synthesis and properties of the selected catalysts.

Entry	Catalyst	Catalyst preparation	Catalyst properties	Metal particle size (nm)	Ref
1	K–CuFe/CNF	Precipitation of Fe and Cu nitrates and dissolving the precipitate with citric acid. Thereafter support and the sol (pH = 3.5) of metals and K_2CO_3 was mixed magnetically at 110 °C for 6 h and dried in air at 110 °C. The catalyst was reduced at 400 °C.	Cu/Fe molar ratio 1.93 : 1, CuFe total content 4.9 wt% STEM-EDX: Fe as Fe_3O_4 -metal particles confined in the hollow cores -the size of Fe was enhanced by K addition H_2-TPD under high pressure: higher amount of hydrogen is desorbed in comparison to CNF catalyst without K	Cu: 11.9 Fe: 4.8	[41]
2	CuFe supported on hierarchical hollow silica spheres (HHSS) (Cu-Fe@HHSS)	Ultrasound assisted co-impregnation of iron and cupper nitrates on hierarchical hollow silica spheres, dried at 110 °C and calcined at 450 °C for 4 h and reduced in situ prior to reaction at 300 °C for 6 h	8.2 wt% Cu, 9.3 wt% Fe HRTEM: XRD: $CuFe_2O_4$ spinel confirmed, Cu–CFe_2C_2 composite in the spent catalyst	Fe, Cu: 2–5	[50]
3	$Cu_4Fe_1Mg_4$ mixed metal oxide	$Cu_xFe_yMg_4$ mixed metal oxide catalysts were prepared using metal nitrates as precursor and a nucleation and aging separation method [64]. The catalyst was calcined at 500 °C for 4 h and reduced with a gas mixture 25% CO, 25% H_2, and 50% CO_2.	Cu/Fe ratio 2.37 CuFe, TEM: Cu + Fe content together is 5 wt%, molar ratio of Cu/Fe = 2, K/(Cu + Fe) ratio is 0.01 Fe_5C_2 particles covering Cu nanoparticles.	Cu 21	[36]
4	K–CuFe supported on hierarchical MFI	Hierarchical MFI was prepared via treating it with aqueous NaOH, followed by ion exchange with NH_4NO_3. The hierarchical zeolite was impregnated with a solution of K_2CO_3 with Cu and Fe nitrates. The catalyst was reduced at 400 °C for 4 h.	Large pores (7.8 nm) in alkali treated MFI zeolite Availability of metals was better in desilicated zeolites Low amount of Brønsted acid sites promoted higher selectivity to higher selectivity to alcohols	16.8	[40]
5	CuFeMn-$GO_{0.3}$ (GO graphene oxide)	The aqueous solution containing an equimolar ratio of Fe, Co and Mn nitrates was dropwise added to dried graphite oxide particles. Thereafter the metal loaded graphite oxide particles were stirred and the mixture was aged at 60 °C for 6 h, dried at 80 °C and calcined at 550 °C for 4 h under N_2.	H_2-TPD: small amount of hydrogen desorbed than in the absence of GO The molar ratio of Fe : Cu:Mn is 1 : 1 : 1. CO TPD: lower amount of CO adsorbed H_2O TPD: lower water adsorption capacity of CuFeMn-GO with an optimized GO content XPS: an optimized GO content gave enhanced Cu and Fe reduction, 66 at% Cu^0 and 33 at% Cu^{2+} as well as 59 at% Fe^0 and 41 at% Fe^{2+}	n.a.	[54]
6	CuZnO	The catalyst was prepared by coprecipitation using Na_2CO_3 and metal nitrates as reagents at 65 °C at pH of 6.5. The precipitate was filtrated, washed, dried and calcined at 330 °C for 3 h.	2 wt% Cu, Cu^{2+} ions embedded into ZnO lattice were promoting formation of CH_x and carbon chain growth	n.a	[37]
7	$CuCoMn_{1.5}$	The multimetallic catalyst was prepared by coprecipitation as follows: Metal nitrates were dissolved in water and mixed with an aqueous solution of NaOH and Na_2CO_3 and stirred at 85 °C for 24 h. Thereafter the solid product was washed and dried and calcined at 400 °C for 5 h. Prior to the experiment the catalyst was reduced at 400 °C for 5 h.	Cu : Co:Mn : Al molar ratio is 1:0.5 : 1.5 : 1 Synergetic effect between Cu + and Co species in the presence of Mn facilitated ethanol formation	7–8	[46]
8	CoCu	The catalyst is prepared using Cu-, Co–Al- and Zn nitrates as precursors and the catalyst was precipitated with NaOH and Na_2CO_3 at 65 °C at pH 9. The precipitate was filtrated, washed, dried and calcined at 350 °C for 3 h.	The molar ratio of Co : Cu:Zn : Al is 40 : 20 : 15 : 25 Spinel phases, such as Co_3O_4 and $ZnAl_2O_4$ were present in the catalyst. Intergrowth of Cu0 and Co2 C phase were observed in the spent catalyst.	n.a.	[33]
9	3Cu5Co/(Mn–Al)	Co- and Mn-nitrates together with citric acid were dissolved in distilled water. Polyethylene glycol (PEG 200) was dropwise added into the solution. Another solution composed of Cu and Co nitrates and citric acid was stirred at 50 °C for 1 h. Thereafter the two mixtures were mixed together and a gel was formed when evaporating the solvent at 80 °C for 2 h. A xerogel was obtained when drying the gel at 120 °C for 8 h. Thereafter it was calcined at 450 °C.	$CuCo_2O_4$ alloy was formed.	5–8	[55]
10	CuCoAlZnOZrO_2	The catalyst was prepared by a coprecipitation method[65]	Cu/Co/Al molar ratio is 1 : 2 : 1, ZnO/ZrO_2 weight ratio is 4 : 1, in the final catalyst the weight ratio of CuCoAl: ZnO/ZrO_2 is 2 : 1 This catalyst facilitated to produce a balanced amounts of CO*, CHx* and H* surface species confirmed by H_2 + CO temperature programmed desorption connected with MS		[34]

Table 2. continued

Entry	Catalyst	Catalyst preparation	Catalyst properties	Metal particle size (nm)	Ref
11	Co_3Cu_1KIT-6	KIT-6 material was synthesized according to[66], copper and cobalt nitrates were dissolved in ethylene glycol and the mixture was stirred overnight, vacuum dried at 120 °C and calcined at 550 °C for 4 h and reduced in situ at 400 °C for 6 h	The total metal loading is 30 wt%. Alloy formation is confirmed Co is well dispersed	4.3	[2]
12	$Cu_{0.25}Co_{0.75}$@C	The mixture of Cu and Co chlorides in ethylene glycol was mixed in an ice bath, Thereafter aqueous $NaBH_4$ was added dropwise in the mixture. The precipitate was washes, dried in vacuum at 60 °C and activated in hydrogen atmosphere at 300 °C.	HRTEM: lattice parameter corresponds to CuCo alloy EXAFS: $Cu_{0.25}Co_{0.75}$ confirmed XPS. Cu 2.36 at%, Co 14.6 at%, Cu/Co molar ratio 0.16, Presence of Co^{2+}, Co^0, Cu^0 prominent with small amount of Cu^+ H_2-TPR: peak shifted to higher temperature (190–480 °C) in comparison to the catalyst with more Cu, the second peak maximum at 480 °C, CoOx is known to be reduced at higher temperature CO-TPD: low temperature peak for desorption of CO from Cu, high temperature peak for strong CO adsorption for CO dissociation	< 10	[45]
13	Cobalt supported on graphene oxide-ordered mesoporous silica (GO-OMS)	Graphene oxide was prepared by oxidation of graphite[67]. Then Pluronic was added into GO suspension and finally hydrolyzed with TEOS. After hydrothermal treatment mesoporous graphene oxide silica composite was formed. Cobalt was loaded via incipient wetness method	The higher alcohol formation was promoted by formation of Co_2C which enhances non-dissociative adsorption of CO 3 wt% graphene oxide and the rest is ordered mesoporous silica in the support. 11.6 wt% Co. Both Co and Co_2C coexisted in the catalyst After 108 h time-on-stream Co_2C decomposed -The benefit with this catalyst was low CO_2 formation	Co 8.6	[29]
14	$Co_{4.7}$Mo@C	$Co_{4.7}$Mo@C catalyst which is derived from polyoxymetalate and Co/Co_6Mo_2C was confined in the carbon matrix[35]	Rhombic dodecahedral structure of the catalyst is confirmed by TEM. Co(Mo molar ratio is 4.7, Co and Mn contents are 31.7 wt% and 10.9 wt%, respectively. The balance between Co^0/Co_6Mo_6C was crucial for selective CO insertion forming higher alcohols Co_6Mo_6C phase confirmed by XRD		[35]
15	Co_1Mn/AC	Cobalt nitrate and manganese acetate were loaded on acidified active carbon via incipient wetness impregnation method. The catalyst was dried and calcined at 350 °C in argon atmosphere.	The syngas treated catalyst contained Co_2C phase. Mn species were well dispersed on the support. K-edge EXAFS showed the coexistence of Co^0 and cobalt oxide species.	18.2	[57]
16	CoFe-300–CNa	α-FeOOH nanorods were coated with carbon with tris(hydroxymethyl) aminomethane buffer solution and dopamine -HCl in water. After washing the material was calcined in H_2 at 400 °C for 4 h. Thereafter Co nitrate was impregnated on carbon coated nanorods and calcined at 350 °C for 4 h in N_2. The catalyst was reduced at 300 °C. Thereafter Na added via mixing an aqueous solution of Co/α-Fe_2O_3 with NaOH, stirring at 80 °C for 12 h and dried, diluted with 4 : 1 ratio with α-Al_2O_3	XRD: the presence of CoFe alloy was confirmed, Fe/Co molar ratio is 7.4. Mössbauer spectroscopy: both CoFe alloy and α-Fe present Notation 300 indicates reduction temperature of 300 °C. SEM-EDX: Co/Fe ratio 7.3, in spent catalyst CoFe bimetallic carbides, XPS charge transfer from Na to Fe_xC strengthens Fe–C bond and weakens C–O bond: the best Na amount 0.25 wt%. Sodium facilitates stabilisation of ε-carbide species CO-TPD: higher desorption temperature for CO with Na addition, CO adsorbed on iron H_2-TPD: increased CO desorption and decreased H_2 desorption temperature results in decreased H_2/CO surface ratio,		[52]
17	RhCoMn	Co-precipitation method was used to prepare Rh–CCo–CMn catalyst using $RhCl_3xH_2O$, with Co- and Mo nitrates as precursors and Na_2CO_3 as a precipitant. Thereafter the precipitate was washed, dried and calcined at 330 °C for 3 h.	1.1 wt% Rh, Co/Mn ratio is 1. H_2-TPR: lower reduction temperature was observed for Mn doped catalyst than for parent one due to hydrogen spillover effect. In situ DRIFTS: stronger CO adsorption promoting reduction and carburization XPS: in fresh catalyst Co^{3+} and Co^{2+} and Rh^{3+}, after reduction Rh^{3+}, Rh^+, in spent catalyst $Rh\delta^+$	n.a.	[44]
18	CoMnOx-quasi-MOF-74	The catalyst was prepared by controlled deligandation of CoMn-MOF-74 at 400 °C for 4 h followed by pyrolysis at 500 °C for 4 h	The content of Co and Mn are 32.1 wt% and 10.5 wt%, respectively. The role of Mn is to promote Co_2C formation which facilitates higher alcohol formation	8.3	[28]

Table 2. continued

Entry	Catalyst	Catalyst preparation	Catalyst properties	Metal particle size (nm)	Ref
			Co/MnO_x nanoparticles are inside quasi-MOF-74 and three different active sites were present in the catalyst, namely Co^0, Co^{2+} and coordinatively unsaturated sites (CUS)		
19	CoMn/CuZnAlZr	Multimetallic catalyst was prepared by coprecipitation method, in which Na_2CO_3 was dropwise added into the solution containing dissolved metal ions, stirred and after aging at 30 °C at pH 8 it was centrifuged. The powder was calcined at 350 °C for 4 h.	The "support " is Cu/Zn/Al/Zr with the molar raito of 2 : 1:0.9:0.1. The content of Co and Mn is 50 % in the final catalyst and Na-content is 1 wt %.According to in-situ DRIFTS measurements CuZnAlZr contains adsorbed CH_xO* species, while the role of Co/Co_2C interface was to promote insertion of CH_3O* into alkyl species forming C_mH_yCHO*[1]		[38]
20	K–CoRhMo supported on carbon nanohorn	Carbon nanohorn was treated with HNO_3, at 110 °C, and rinsed with de-ionized water, treated with aqueous solution of K_2CO_3, followed by heat treatment in argon at 300 °C. Metals were loaded via co-impregnation (Rh chloride hydrate, ammonium heptamolybdate tetra hydrate, cobalt acetate)	Elemental composition: 4.2 wt % Co, 15.1 wt % Mn, 1.3 wt % Rh, large surface srea 499 m^2/g_{cat}[25]	MoO_3: 6–10	[25]
21	K–$NiMoS_2/Al_2O_3$	Ammonium heptamolybdate dissolved in water and NH_4OH was added into this solution followed by KOH addition. Thereafter this solution was added into the solution containing nickel acetate tetrahydrate and citric acid. Al_2O_3 was impregnated with this solution and dried. Prior to the experiment the catalyst was sulfided.	Potassium addition reduced number of metal atoms in $NiMoS_2/Al_2O_3$ and also oxophilicity of the catalyst, which in turn increases insertion of CO into metal-carbon bond of surface alkyl intermediate	n.a.	[4]
22	K–MoS_2	Molybdenum sulfide was prepared using ammonium molybdate and sodium sulfide as precursors and stirring these in the presence of 4 % hydrochloric acid solution. Thereafter hydroxylamine hydrochloride was added into the solution. The slurry was filtered and washed with deionized water and K_2CO_3 was added to the catalyst via physical mixing with a mortar.	K/Mo molar ratio is 0.22. The physical mixing of catalyst and K_2CO_3 resulted in formation of multilayers of MoS_2 and $KMoS_2$, which promote C3 + alcohol formation	n.a.	[5]
23	K–MoS_2–Mn–Al composite	An aqueous solution containing Mn-and Al-nitrates with citric acid polyethylene glycol 400 (PEG 400) was added dropwise and stirred for 1 h. To another solution containing K-nitrate and ammonium molybdate citric acid was added and the solution was stirred at 65 °C for 1 h. Thereafter the two prepared solutions were mixed together and the solvent was evaporated under mild stirring at 80 °C. The resulting gel was dried at 120 °C. Thereafter the dried gel was treated with non-thermal plasma containing with H_2S.	K/Mo ratio is 3/5. Small slabs (MoS_2) were present in the catalyst. In situ DRIFTS showed that non-dissociative adsorption of CO was promoted over this catalyst.	7.7	[56]
24	$RhKMo_2C$	Rh-nitrate in aqueous solution was loaded on Mo_2C support via impregnation. Thereafter KOH solution was added dropwise to the catalyst slurry. The catalyst was dried at 120 °C for 6 h under vacuum drying and reduced in situ with a syngas flow at 300 °C for 2 h.	Elemental composition: 1.6 wt Rh, 4.8 wt % K., 70.3 wt % Mo. K promotor enhanced Rh dispersion Rh^{d+} species facilitated non-dissociative adsorption of CO	n.a	[48]
25	KMoP/mesoporous carbon	K was first impregnated to the mesoporous carbon support via incipient wetness method, the modified support was dried and calcined at 120 °C and 500 °C, respectively. Ammonium heptamolybdate and diammonium hydrogen phosphate were dissolved in deionized water and this solution was dropwise added via incipient wetness method to the support, mesoporous K-modified commercial carbon (Starbon).	Elemental composition: 1.1 wt % K, 15 wt % Mo. The presence of MoP was confirmed by EXAFS. In addition to reduced MoP also unreduced Mo phosphate phase was present Slight sintering of Mo particles found by EXAFS, however, not affecting catalytic performance	5–6	[47]
26	Au–CFe_3O_4	Gold nanoparticles were prepared from gold chloride trihydrate which was mixed with tetraline under Ar. Tert-butylamine (TBAB) and oleylamine (OAm) were injected into Au solution and mixed at 4 °C. Thereafter they were precipitated by ethanol. These gold nanoparticles were mixed with a solution containing Fe(oleate) and OAm and it was refluxed at 320 °C. for 30 min. After	Elemental composition: 5.4 wt % Au, 5.7 wt % Fe, Fe/Au molar ratio is 11.6. The carburized Au and Fe particles were 6.7 nm and 13 nm. The metal particles exhibited Janus structure. Mössbauer spectroscopy: Carburized catalyst contained $\varepsilon'Fe_{2.2}C$ in Au–CFe10 catalyst CO-TPD: the lower peak associated to non-	Au: 5.4 nm Fe_3O_4 12 nm	[53]

Table 2. continued

Entry	Catalyst	Catalyst preparation	Catalyst properties	Metal particle size (nm)	Ref
		cooling and ethanol addition the Au–CFe_3O_4 nanoparticles were separated, washed and dispersed in hexane. Finally they were supported on α-Al_2O_3 which was prepared via calcination of pseudo-boehmite at 1200 °C. The loading of nanoparticles was performed in mixing the nanoparticles with support in hexane and evaporating hexane.	dissociative CO increased with decreasing iron content, while the high temperature peak in CO-TPD connected to CO dissociative desorption increased with increasing iron content. In situ DRIFTS: different intermediate species adsorbed on catalyst as a function of time facilitates to propose reaction mechanism		

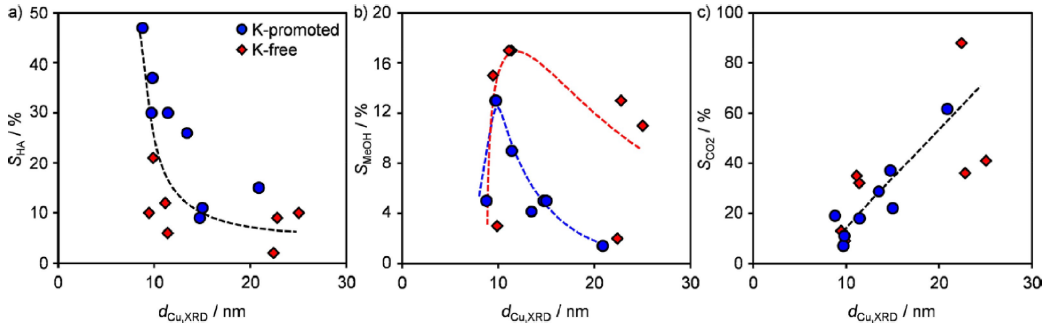

Figure 5. Selectivity to a) higher alcohols, b) methanol and c) CO_2 as a function of the metal particle size determined by XRD over different types of K–CuFe/CNF catalysts. Reproduced from ref. [41] Copyright (2018) with permission from American Chemical Society.

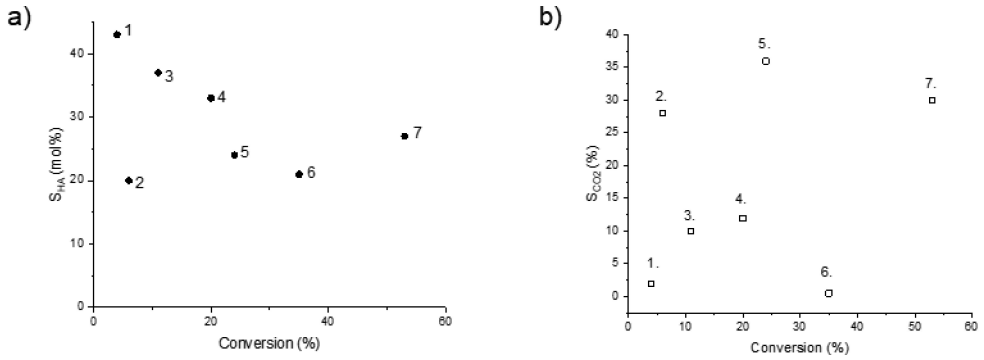

Figure 6. Selectivity to a) higher alcohols (●) and b) CO_2 (■) in transformation of syngas over different catalysts. Notation: 1) K–CuFe supported on hierarchical MFI,[40] 2) CoCu,[33] 3) K–CuFe/CNF,[41] 4) Au–CFe_3O_4,[53] 5) K-MoS_2,[5] 6) Co-graphene oxide mesoporous silica composite[29] and 7) $Cu_4Fe_1Mg_4$-layered double hydroxide.[36]

important role of Co_2C in enhancing higher alcohols formation. Analogously to the results of,[29] extremely low CO_2 amounts were reported over Co_3Cu_1KIT-6 exhibiting very small Co particles (Table 1, entry 11, Table 2, entry 11).[2] The same was reported also for $Cu_{0.25}Co_{0.75}$ with small metal particles.[45]

For cobalt containing catalysts the largest formation of higher alcohols was observed for sodium promoted CoFe alloy,[52] in which hydrogenation and chain growth functions are optimized for higher alcohols. It was stated that especially the role of sodium was to enhance formation of a specific ε′-$(Co_xFe_{1-x})_{2.2}C$ carbide confirmed by XRD which modulates synthesis of higher alcohols. Furthermore, generation of higher alcohols was also promoted over RhCo–Mn oxide catalysts due to the presence of the Co^0–Co_2C–$Rh^{\delta+}$ phase.[44] The role of Co^0 is to dissociate CO and facilitate coupling of C–C to form alkyl species,[44] while Mn influences the cobalt carbide phase, which diminishes hydrogenation ability and chain termination.[44] A rather high space time yield of alcohols was also obtained with $CoMnO_x$-quasi-MOF-74 (Table 1, entry 19).[28] The role of Mn is to prevent metal agglomeration, thus the metal particle size in the pyrolyzed $CoMnO_x$-quasi-MOF-74 was ca. 8 nm (Table 2, entry 18). During pyrolysis the specific surface area was greatly retained, however, nanoparticles emerged during pyrolysis. The distance between Co^{2+} ions in the MOF structure is elongated in the presence of Mn.[28] Furthermore, Mn promotes CO insertion[28] resulting in very low amounts of CO_2 and CH_4 (see

below). In addition to the Co_2C sites, Co^{2+} sites present in the MOF framework were considered beneficial for formation of higher alcohols (Table 2, entry 19).[28] In another work[46] it was, however, stated that the interplay between Cu^+ and Co in $CuCoMn_{1.5}$ catalyst resulted in mainly ethanol. Multimetallic CoMn/CuZnAlZr was very selective to formation of higher alcohols (Table 1, entry 19, Figure 7).[38] which was related to formation of CH_xO* species (Table 2, entry 19) confirmed by DRIFTS measurements. These species migrated to the Co/Co_2C interface facilitating insertion of alkyl species and formation of C_mH_yCHO*. Analogously in another study the Co–Co_2C interface was considered to promote alcohols formation.[57] Furthermore, multimetallic Cu–Co/(Mn–Al) catalyst containing Cu–Co alloy was efficient for higher alcohols formation with both Cu and Co required for hydrogenation and insertion of alkyl species.[46]

A bimetallic Co_3Cu_1 supported on KIT-6 with a small metal particle size (Table 2, entry 11) was quite selective towards alcohols affording 46% selectivity at 63% conversion (Table 1, entry 11).[2] Another CoCu catalyst gave ca. 20% selectivity to higher alcohols (Figure 6a), however, with this catalyst some sintering was confirmed by XRD resulting in high selectivity to the undesired CO_2 (Figure 6b).[33] Analogously the small metal particles in 20 wt% MoP–K/SiO_2 were beneficial for the lowest formation of CO_2.[47] K–Rh/Mo_2C exhibited 44% selectivity to higher alcohols under 1.0 MPa (Table 1, entry 24).[48] It was stated that high dispersion of Rh, present partially as Rh^{d+} facilitated further formation of olefins. Additionally, K–CNiMoS2 was also very selective to formation of alcohols (Table 1, entry 21).[4] The role of K was to suppress hydrogenation ability resulting in formation of very low amounts of hydrocarbons, while formation of large amounts of CO_2 could not be avoided.

A bifunctional CuZnO with Cu as a hydrogenating element and ZnO promoting the chain growth was also an efficient catalyst for production of higher alcohols (Table 1, entry 6).[37] When ZnO was doped with Cu present in the optimum amounts (4 mol%) the highest molar ratio of $C_{2+}OH/ROH$ of ca. 50% was obtained.

In syngas transformations, in addition to higher alcohols, also other products, such as methane and higher hydrocarbons as well as alkenes and traces of aldehydes are formed.[41] Large differences in α-value were observed when changing the composition of bimetallic catalysts,[36] e.g. the ratio between Cu and Fe. The highest α-value for the alcohol formation was seen for $Cu_4Fe_1Mg_4$ on mixed metal oxides catalyst, being 0.72 at 1.0 MPa at 260 °C (Table 1, entry 3), while for Cu_1Fe_4 it was only 0.55.[36] These results were explained by the highest concentration of interfacial Fe_5C_2–Cu sites present in the catalyst confirmed by CO-temperature programmed desorption techniques and quasi-in situ scanning transmission electron microscopy.[36] Typically, both hydrocarbons and alcohols are formed as the main products (Table 1) with their distribution being defined by two respective α-values.[28,32,35,44,47] In some cases a higher α-value has been obtained for alcohols compared to hydrocarbons (Figure 8)[34,36] indicating that CO insertion is faster than the hydrocarbon chain termination.

The effect of temperature and pressure on the chain growth will be discussed below. One example showing the product distribution in syngas transformations over $CoMnO_x$ quasi MOF-74 to higher alcohols and hydrocarbons as a function of the carbon number at two values of α is given in Figure 9. It was stated[28] that the Anderson-Schultz-Flory product distribution often reported in different polymerization processes as well as in the Fischer-Tropsch synthesis was valid for C3+ alcohols. A high ratio of C_{3+OH}/ROH (53%) was obtained over $CoMnO_x$ quasi MOF-74 catalyst under 3.0 MPa at 200 °C with the CO/H_2 ratio of 0.5 and gaseous hourly space velocity of 4500 ml/(g_{cat}h) at ca. 22% conversion.[28]

The undesired water gas shift reaction forming CO_2 has been suppressed by using K–CuFe supported on hierarchical MFI zeolite,[40] $CoMnO_x$[28] CuCo,[2,38,45] $CuCoMn_x$ (Figure 10)[46] and CuFe type catalysts,[54] while rather high amounts of CO_2 were formed over Cu_4Fe_1,[36] CuZnO[37] and multimetallic CuCoAlZnOZrO[34] and with CoMn/CuZnAlZr[38] (Table 1). It can, however, be seen from Table 1 that over CoMn/CuZnAlZr the main alcohol formed is ethanol.

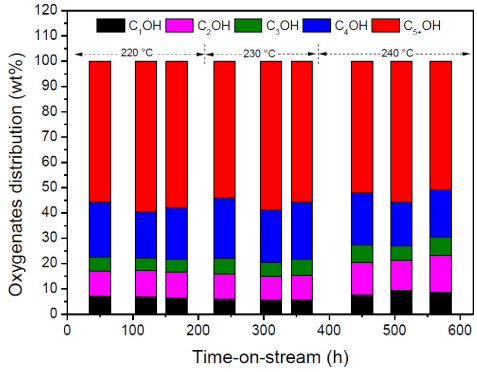

Figure 7. Distribution of alcohols in syngas transformations to higher alcohols over CoMn/CuZnAlZr catalyst under 6.0 MPa with H_2:CO ratio of 1 and WHSV of 2000 ml/$g^{-1}h^{-1}$. Reproduced from ref. [38] Copyright (2019) with permission from Wiley and Sons.

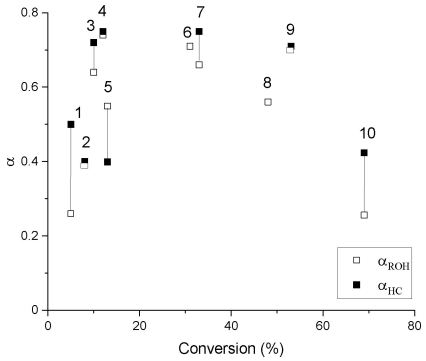

Figure 8. Chain-growth probability a calculated on the weight basis from eq. (4) for different catalysts in syngas transformations to alcohols and hydrocarbons as a function of conversion. Notation: 1) 1.1Pd–K-MoP/SBA-15,[47] 2) CoCu,[32] 3) $CoMnO_x$,[28] 4) CoMnCuZnAlZr,[38] 5) $CuCoAlZnOZrO_2$,[32] 6) CoFe-300–CNa,[52] 7) 1.1Rh–CoMn,[44] 8) Cu_4Fe_1,[36] 9) $Co_{4.7}Mo@C$,[35] and 10) 4CuZrO,[37] lines between α_{ROH} and α_{HC} indicate the same values for one catalyst.

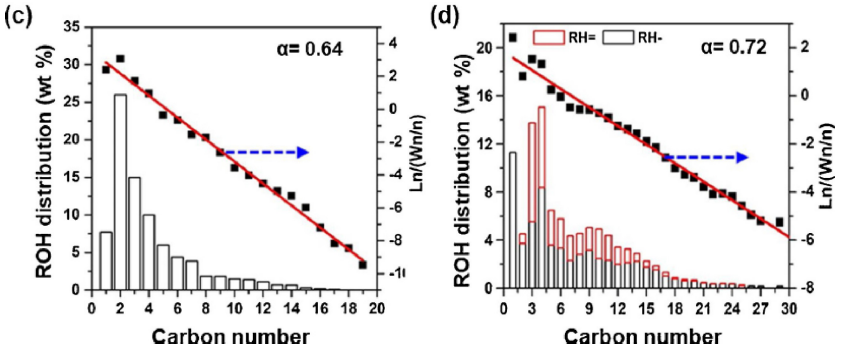

Figure 9. Alcohol and hydrocarbon distribution in syngas transformation over Co/MnO_x quasi-MOF-74 under 3.0 MPa at 230 °C with CO/H_2 ratio of 1 : 2 and gas hourly space velocit /y (GHSV) of 4500 ml/(g_{cat}h) after TOS = 24 h, a) α = 0.64, b) α = 0.72. Reproduced from ref. [28] Copyright (2020) with permission from Elsevier Ltd.

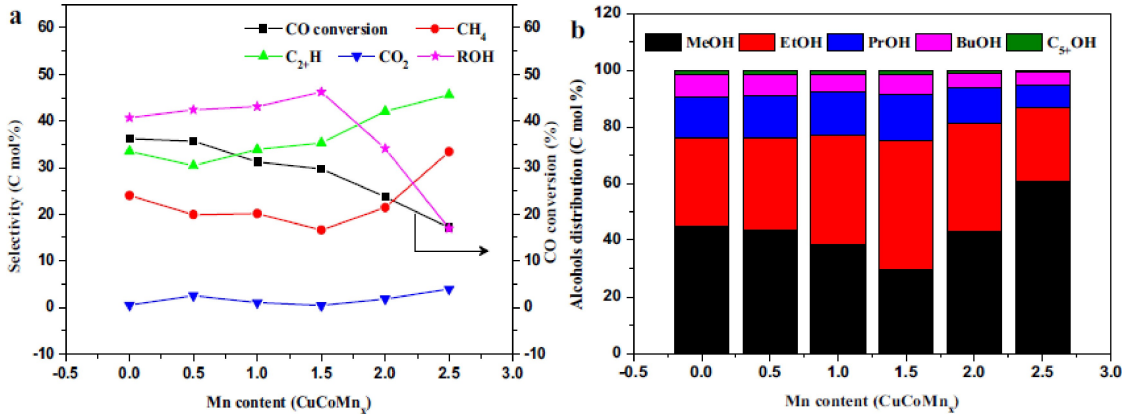

Figure 10. Syngas transformation to higher alcohols over CuCoMn catalysts as a function of Mn content a) product and b) alcohol distribution. Conditions: 2.5 MPa, 270 °C, gas hourly space velocity 700 h^{-1}. Reproduced from ref. [46] Copyright (2019) with permission from Elsevier Ltd.

The water gas shift reaction and formation of CO_2 were suppressed over CoMn/$CuZnAlZrO_2$[38] and CuFeMn-GO.[54] It was also interesting to observe that a lower amount of water was desorbed in H_2O TPD for CuFeMn-GO (GO denotes graphene oxide) with an optimized graphene oxide content, which facilitated a shorter contact time for water on the catalyst surface and suppressed the water gas shift reaction producing CO_2.[54] For CoFe–CNa catalyst a higher desorption temperature for CO and on the contrary a lower desorption temperature for H_2 resulted in a lower H_2/CO surface concentration ratio suppressing the water gas shift reaction.[52] Very low amounts of CO_2 were formed over bimetallic CoCu supported on KIT-6 with a small metal particles size (Table 1, entry 11). An optimum CoCu ratio was reported to be 4 : 1, while with an increasing copper content more methanol was formed,[2] suggesting that higher alcohols formation can be achieved with an optimum Co loading.

4. Catalyst Activation, Thermodynamics and Effect of the Reaction Conditions

4.1. Catalyst Activation

Typically catalyst activation after its reduction with syngas is required to produce initially higher alcohols. An induction period was also observed when the catalyst was activated in the presence of syngas and CO_2.[36] If only a reduced catalyst, e.g. CoCu, is used with syngas, higher alcohols can be obtained after an induction period[32,33] and the steady state was obtained at 280 °C under 6.0 MPa with the H_2:CO ratio of 1 after 40 h.[32] Furthermore, it was concluded in[33] that under the steady state conditions intergrowth of Cu^0 with Co_2C was observed. When a catalyst is activated with syngas,[44] CO[53] or syngas and CO_2 mixture,[36] higher alcohol production starts at a shorter time-on-stream. It has also been reported in[35] that the presence of Cu–CFe_2C_2 interfacial sites with an intimate contact facilitates formation of higher alcohols. When activating the Cu–Fe catalyst in the presence of CO_2, it was observed by XRD that the interfacial phases containing Cu–Fe_5C_2 were formed, being selective to higher alcohols formation.

4.2. Thermodynamics for Higher Alcohol Formation from Syngas

Thermodynamic analysis, being important for design of industrial processes, has been scarcely performed for transforming syngas to alcohols, C1–C4.[68–70] In[70] equilibrium concentrations were calculated for alcohols formation and the water gas shift reaction. Evaluation of the maximum yields of various products for CO and H_2 feeds of 0.3 and 0.7 molar fractions under 3.0 MPa revealed that butanol is the main product with the molar fraction of 0.78 at 277 °C followed by propanol with 0.18 (Figure 11). On the other hand, CO_2 content from the water gas shift reaction is 0.04 while the ethanol fraction should be very low. An apparent discrepancy with the experimental data reporting high yields of ethanol, indicates kinetic rather than the thermodynamic control. With increasing temperature up to 477 °C the corresponding predicted molar fractions are: 0.46 for butanol, 0.2 for CO_2, 0.16 for propanol and 0.03 for ethanol.[70] The highest equilibrium amounts of butanol can be obtained at high pressures, e.g. 5.0–7.0 MPa corresponding to 0.78, while at a lower pressure of 3.0 MPa the butanol fraction is 0.7. Furthermore, CO_2 generation by the water gas shift reaction exhibits the highest level at 3.0 MPa being 0.2 at 477 °C, while at higher pressures, the CO_2 fraction remains at ca. 0.2 at 477 °C (Figure 11).

In the thermodynamic analysis of[69] equilibrium composition was calculated by minimization of total Gibbs free energy using the Peng-Robinson equation and taking into account elemental balances considering[68] only C1–C4 alcohols, because C5+ alcohols were minor products. According to[69] the main products were C4 alcohols at 300 K, while their amounts decreased with increasing temperature under 7.0 MPa with the H_2/CO ratio of 2 (Figure 12c). The opposite was found for formation of methanol, as its formation is less exothermic than that of the higher alcohols. Furthermore, CO_2 formation was exponentially enhanced above 500 K. Tert-butanol is the main product among C4 alcohols at 300 K, while 2-butanol becomes a more prominent product at 470 K (Figure 12c). When comparing the results of[69] with the H_2/CO ratio of 2 to those of[70] with the H_2/CO ratio of 2.3 at 550 K under 7.0 MPa, it can be seen that the C4 alcohol fractions were 0.95 and 0.79, respectively, which is probably related to different models applied in these studies. Despite these differences, a common conclusion from both studies is that with a higher H_2/CO ratio less alcohols should be formed.

Furthermore, it was reported in[71] that the thermodynamically most favorable product in syngas transformation is methane, followed by paraffin and alcohols formation:

$$\begin{aligned} &CH4 > \text{paraffin} > \text{i-BuOH} > \text{n-BuOH} \\ &> \text{n-PrOH} > \text{EtOH} > \text{MeOH} \end{aligned} \tag{8}$$

It can be concluded based on these results that the production of higher alcohols is limited at high temperatures, although high conversion of H_2 and CO can be obtained at 600 K being 90 % and 100 %, respectively.

4.3. Effect of Reaction Conditions

The effect of reaction conditions, such as temperature, pressure, contact time and the H_2/CO ratio has been intensively studied for production of higher alcohols, as they can have a major effect on the reaction rate and product distribution, for example on the chain growth probability,[36,42,72] methanation and CO_2 formation.[52]

4.3.1. Effect of Temperature

In synthesis of higher alcohols from syngas an adequate balance should be found between the reaction kinetics, affected especially by temperature, and thermodynamics. Higher alcohols formation is thermodynamically favored at lower temperatures, e.g. at ca. 270 °C[70] as discussed more above. The effect of temperature on the higher alcohol formation has been intensively studied experimentally[4,5,25,27,33,35–37,40–42,45,48] reporting values of the activation energies for synthesis of different hydrocarbons and alcohols in syngas transformation over

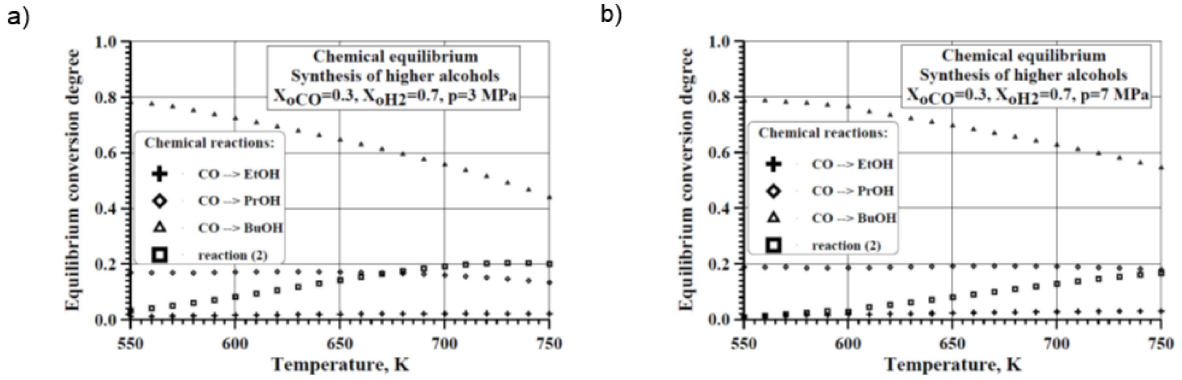

Figure 11. Equilibrium conversion for formation of butanol, propanol and ethanol as a function of temperature at a)3 MPa and b) 7 MPa.[70] Notation: Reaction (2) is the water gas shift reaction. Reproduced from ref. [70] Copyright (1999) with permission from Elsevier Ltd.

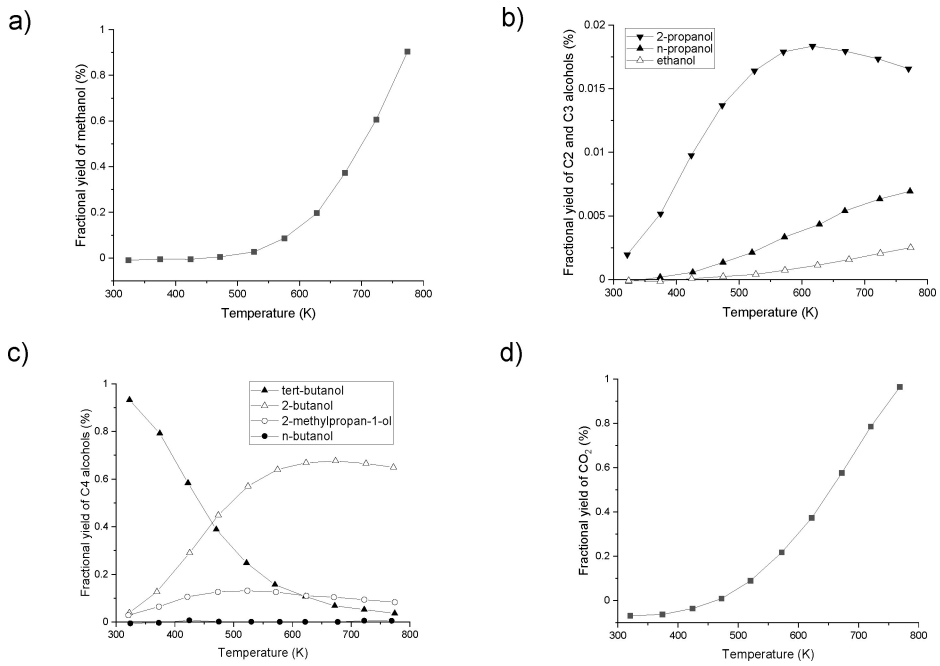

Figure 12. Calculated equilibrium fractions of a) MeOH, b) ethanol and C3- alcohols, c) C4 alcohols and d) CO_2 adapted from ref. [69]. Conditions: H_2/CO ratio of 2, 70 MPa.

2CoCu catalyst,[32] Co-MoS_2-K_2CO_3,[42] K–CoRhMo supported on carbon nanohorn[25] and K–CoRhMo/MWCNT.[73]

Over CoFe–CNa supported on α-FeOOH nanorods, the reaction rate was enhanced with increasing temperature and at the same time conversion and selectivity to CO_2, methane and alkanes increased, while selectivity to ROH and olefins exhibited maxima.[52] Analogously a maximum selectivity to alcohols was observed for K–CuFe/CNF catalyst (Figure 13).[41] On the other hand, selectivity to alcohols decreased with increasing temperature over CuCoMn catalyst (Figure 14)[46] analogously to Co/MnO_x@C.[35]

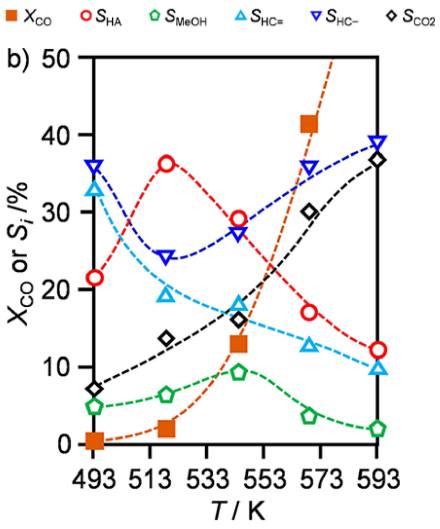

Figure 13. The effect of temperature in transformations of syngas to higher alcohols over K–CuFe/CNF catalyst under 5.0 MPa with H_2/CO ratio of 2 and gas hourly space velocity of 16000 $cm^3/(g_{cat}h)$. Reproduced from ref. [41] Copyright (2018) with permission from ACS publications.

Chain growth probability for alcohol formation for the optimized catalytic systems (Table 1) with the α-value of 0.72 was obtained at a lower temperature of 260 °C over $Cu_4Fe_1Mg_4$ mixed metal oxide[36] while 0.56 was obtained at 275 °C over $Co_{4.7}$Mo@C[35] showing that high temperatures should be avoided for Co- and Cu-based catalysts. Chain-growth probability decreased with increasing temperature for alcohols when increasing temperature from 340 °C to 360 °C and finally to 380 °C as follows: 0.13, 0.11 and 0.09, respectively for cobalt-molybdenum sulfide catalyst promoted with K_2CO_3.[41] Analogously it was confirmed that the chain growth probability for higher alcohols decreased above 267 °C over CoCu/SiO_2 catalyst (Figure 15).[30] Based on these results it can be concluded that the chain termination has a higher activation energy than the chain growth.

4.3.2. Effect of Pressure

The pressure having a large impact on formation of higher alcohols from syngas, has been intensively studied in the literature.[23,24,32,36,41,42,44,48,52] Space time yield of alcohols increased with increasing pressure from 3 MPa to 5 MPa at 260 °C over CoFe-300 (300 denotes reduction temperature) catalyst.[52] As a comparison an optimum pressure of 5.0 MPa was observed for maximizing selectivity to higher alcohols over K–CuFe/CNF catalyst (Figure 16a),[41] while at the same time when increasing the pressure from 3 to 5 MPa, CO_2 and hydrocarbon selectivity

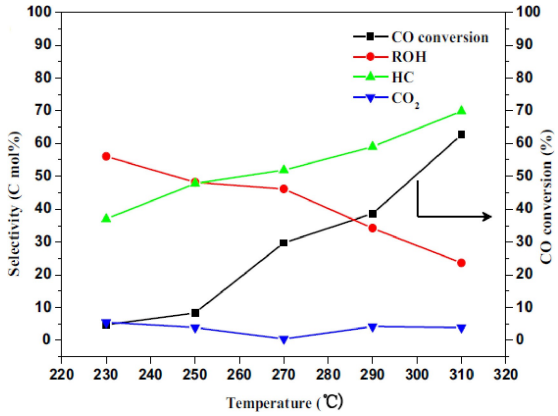

Figure 14. The effect of temperature on product selectivity and CO conversion in syngas transformations over CuCoMn catalyst under 2.5 MPa. Reproduced from ref. [46] Copyright (2019) with permission from Elsevier Ltd.

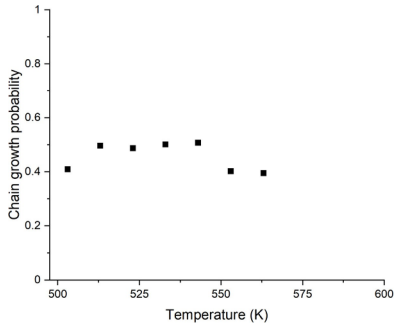

Figure 15. Chain growth probability for formation of higher alcohols over CoCu/SiO_2 catalyst under 5.0 MPa with gas hourly space velocity of 14000 h^{-1} at 30 h time-on-stream with the feed composed of H_2/CO/N_2 of 6:3:1.[30]

increased from 4% to 9% and 7% to 14%, respectively. Analogously an optimum pressure was observed for K–Co–MoS_x catalysts promoting higher alcohols formation (Figure 16b).[42]

An optimum pressure for higher alcohols formation cannot be explained solely by thermodynamics. Thus, the intrinsic kinetics defines the relevance of different competing routes. It was also stated that when CO conversion increases under high pressure, selectivity was only slightly affected by a change of the total pressure over CoCu catalyst.[30] It was, however, reported that the lower threshold pressure to suppress methanation is 3 MPa, above which higher alcohols selectivity was slightly enhanced. CO_2 formation was also increased at higher CO conversion levels for lower H_2/CO ratios.[31] On the other hand, the highest selectivity to higher alcohols was obtained under the lowest pressure over $Cu_4Fe_1Mg_4$ catalyst in.[31] Interestingly, higher selectivity to alcohols was found for CoMn/CuZnAlZr catalyst upon increasing pressure, while lower selectivity to olefins is easily explained by their hydrogenation to alkanes (Figure 17).[37] Selectivity to higher alcohols increased from 46% to 57% when increasing pressure from 1 MPa to 4 MPa, respectively at 290 °C with H_2/CO ratio of 1 for RhK/Mo_2C.[47] It was, however, stated that although Mo_2C based catalyst requires high pressures, a relatively high alcohol selectivity was achieved already below 1 MPa.

4.3.3. Effect of H_2/CO Ratio

The effect of H_2/CO ratio on production of higher alcohols from syngas has been intensively studied.[32,34,36,41,42,44,47] Selectivity to C2+ alcohols decreased from 21% to 16% when conversion increased from 5% to 17% with increasing the H_2/CO ratio over 2CoCu catalyst (Figure 18).[32] Analogous results were reported for K–CuFe/CNF,[41] K–$CoMoS_x$[42] and MoP–K/SiO_2 catalysts.[47]

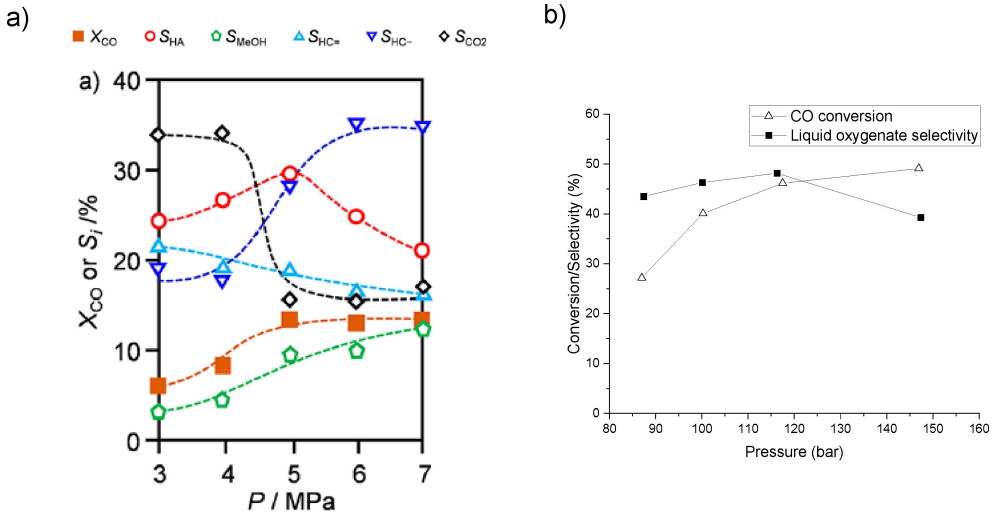

Figure 16. Effect of hydrogen pressure on selectivity to higher alcohols over a) K–CuFe/CNF at 270 °C with H_2/CO ratio of 2 and gas hourly space velocity of 16000 ml/(g_{cat}h). Reproduced from ref. [41] Copyright (2018) with permission from ACS publications and b) K–$CoMoS_x$. Reaction conditions: gas hourly space velocity 4500 ml/(g_{cat}h), 380 °C, H_2/CO = 1. Adapted from ref. [42].

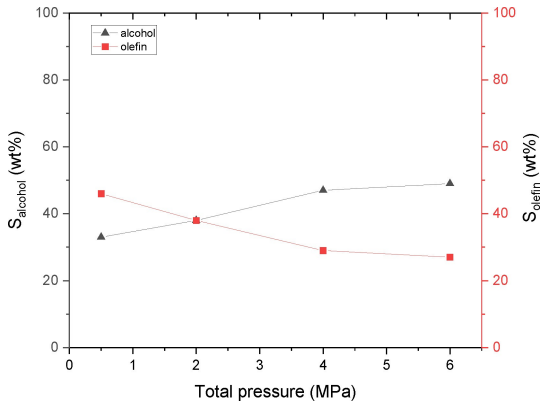

Figure 17. Effect of pressure on alcohol and olefin selectivity in syngas transformations over CoMn/CuZnAlZr catalyst at 230 °C, H_2/CO ratio of 2, weight hourly space velocity 2000 ml/(g_{cat}h). Adapted from data given in ref. [37].

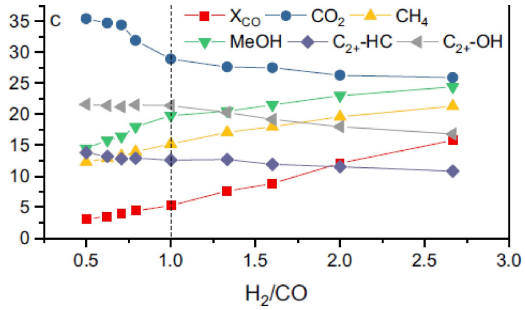

Figure 18. Selectivity changes vs time-on-stream in syngas transformation to higher alcohols over CoCu catalyst under 60 bat at 280 °C with GHSV of 12000 h^{-1}. Reproduced from ref. [32] Copyright (2021) with permission from Elsevier Ltd.

Especially methane formation was enhanced[32,41] when using high H_2/CO ratios while the alkene formation was suppressed.[41,47]

4.3.4. Effect of Contact Time

Typically with increasing gas hourly space velocity (GHSV) conversion decreases and at the same time selectivity to higher alcohols and olefins increases while the opposite is valid for methane, CO_2 and hydrocarbons.[24,32,40–42,44,46,48] These results indicate that CO insertion occurs rapidly, while hydrogenation and dehydration are slower.[41] On the other hand, for Co/MnO_x-quasi-MOF-74 selectivity to alcohols was nearly unaffected by the change of gas hourly space velocity in the range of 4500–15000 ml/(g_{cat}h) at 230 °C with H_2/CO ratio of 2.[28] In general for such catalysts where the active sites were inside the support matrix[28] selectivity can be dependent on diffusion, as reported for carbon nanotubes.[41]

4.3.5. Catalyst Stability

In general very stable catalytic performance in syngas transformation to higher alcohols was reported,[28,41] although in some cases slight deactivation occurred after prolonged TOS.[29]

A long term stability test for 100 h time-on-stream of K–CuFe/CNF was performed at 275 °C under 5.0 MPa with 32000 cm^3/(g_{cat}h) using the H_2/CO ratio of 1.5. Selectivity to higher alcohols remained constant during this experiment being 37% at CO conversion of 14%.[41] At the same time the methanol to higher alcohols ratio was 0.19. It was pointed out that this result was obtained when CO_2 selectivity was only 10%. Very promising performance was found for Cu_4Fe_1 supported on layered double hydroxide, for which after the initial induction period of 10 h the conversion of CO decreased from 51% to 48% up to 100 h time-on-stream at 1.0 MPa.[36] This catalyst was also quite selective giving 1.8 fold higher space time yield of alcohols, in comparison to hydrocarbons.

Minor catalyst deactivation occurred for cobalt supported on graphene oxide -ordered mesoporous silica composite[29] despite a partial decomposition of Co_2C phase during reaction leading to inactive Co_{hcp} phase after 108 h time-on-stream. The bimetallic CoFe-300 catalyst was stable after 60 h giving 45% CO conversion up to 200 h in syngas transformation at 260 °C under 3.0 MPa with the H_2/CO ratio of 2 and gas hourly space velocity (GHSV) of 10800 ml/(g_{cat}h).[52] It was also stated that higher alcohols generation was promoted after formation of the carburized CoFe alloy, which is beneficial for a synergy between CO dissociation and insertion. The phase separation in the carburized alloy is inhibited by cross diffusion of Co and Fe.

Over CoCu catalyst the steady state operation was obtained after ca. 40 h of TOS giving 20% selectivity to higher alcohols at 6% CO conversion (Figure 19).[33] It was stated that strong initial deactivation is due to carburization when Co_2C is formed. Analogously to[31] a stable operation was observed for syngas transformation over CoCu/KIT-6 after 24 h time-on-stream with

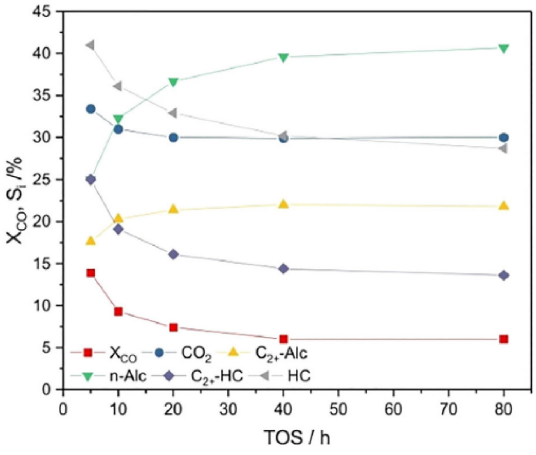

Figure 19. Conversion of CO and selectivity to different products as a function of TOS in transformation of syngas to higher alcohols at 280 °C under 6.0 MPa with H_2/CO ratio of 1 and with the feed rate of 12000 Nml(g_{cat}h) over Co–Cu catalyst. Reproduced from ref. [33] Copyright (2020) with permission from Elsevier Ltd.

very low amounts of CO_2 formed (Table 1, entry 12).[2] A slight catalyst deactivation occurred for 8Co/(MnAl) catalyst at 260 °C under 5 MPa and gas hourly space velocity of 5000 h^{-1} during 200 h time-on-stream.[57] However, the metal particle size increased only from 5.6 to 7.0 nm during this test and Cu–Co alloy remained rather stable on Mn–Al support.

Superior stability of Au–Fe/Al_2O_3 catalyst was observed during 216 h TOS in syngas transformations to higher alcohols at 260 °C under 3.0 MPa with the H_2/CO ratio of 1 and GHSV of 4800 ml/(g_{cat}h).[53] High stability of this catalyst was connected to electronic interactions between Au and Fe particles, which could prevent their aggregation.

Molybdenum containing catalysts have been also quite stable in higher alcohols synthesis.[5,35] Although K-MoS_2 was rather stable with a steady state CO conversion being ca. 20%, selectivity to oxygenates and hydrocarbons was 33% and 32%, respectively while higher selectivity to CO_2 of 36% was also observed.[5] A stable catalyst performance was also reported for $Co_{4.7}$Mo@C catalyst derived from polyoxymetalate where formation of Co/Co_6Mo_2C phase confined in the carbon matrix was confirmed by XRD.[35] This phase was stable after 100 h time-on-stream.

Multimetallic $CoMnO_x$/CuZnAlZr on quasi MOF-74 exhibited also high stability giving a high fraction of C_{3+OH} among alcohols (53%) under 3.0 MPa at 200 °C with CO/H_2 ratio of 0.5 and gaseous hourly space velocity of 4500 ml/(g_{cat}h) at ca. 22% conversion.[28] This catalyst comprised Co^0 and coordinatively unsaturated Co^{2+} sites. Additionally, Co/MnO_x quasi-MOF-74 with two types of active sites, Co_2C and Co^{2+} in MOF framework, was tested for 120 h at 230 °C and 250 °C under 3.0 MPa using the H_2/CO ratio of 2 and gas hourly space velocity of 15000 ml/(g_{cat}h). This catalyst displayed stable performance up to 120 h time-on-stream.[28]

Analogously multimetallic CoMn/CuZnAlZr catalyst was also very stable in syngas transformation between 50 h and 200 h TOS under 6.0 MPa and the H_2/CO ratio of 2 at 220 °C.[38] The ratio between the alcohol to hydrocarbon selectivity in wt% was 1.1 and low selectivity to CO_2 and methane, being 6% and 4%, respectively, was obtained. A very stable performance of $CuCoMn_x$ was additionally observed in syngas transformation giving 30% CO conversion at 270 °C under 2.5 MPa with gas hourly space velocity of 7500 h^{-1}, however, selectivity to hydrocarbons (52%) was higher than for alcohols (47%). On the other hand, selectivity to CO_2 was close to zero.[46]

4.3.6. Kinetic Modelling

In assessing kinetic data and subsequent modelling it is important to ensure that the experiments are conducted in the kinetic regime in the absence of external and internal mass transfer limitations. For elucidation of the external mass transfer limitations, the boundary layer thickness for diffusion of the reactants from the bulk to the active sites was estimated using the following equation:[25]

$$\delta = \frac{D_e}{k_C} \tag{9}$$

in which k_C is the mass transfer coefficient relating the resistance to the mass transfer from the boundary layer and D_e is the effective diffusion coefficient. As well known the boundary layer thickness δ can be minimized by using small particles or increasing the fluid velocities. In[25] the particle size ensuring elimination of the external mass transfer for synthesis of higher alcohols was determined to be 0.088 mm. For suppressing internal mass transfer limitations the Weisz-Prater criterion was applied.[25] Unfortunately there are only a few recent studies in which the kinetic regime of higher alcohols synthesis has been adequately confirmed[25,42,72] and they will be discussed below regarding the reaction orders and kinetic behaviour.

Direct methanol formation from syngas is typically considered:

$$CO + H_2 \rightarrow CH_3OH \tag{10}$$

While methane can be formed either by hydrogenation of CO [eq. (8)] or methanol:

$$CH_3OH + 2H_2 \rightarrow CH_4 + H_2O \tag{11}$$

Thereafter higher alcohols are formed via a stepwise chain growth and CO insertion:

$$CH_3OH + CO + 2H_2 \rightarrow C_2H_5OH + H_2O \tag{12}$$

$$C_2H_5OH + CO + 2H_2 \rightarrow C_3H_7OH + H_2O \tag{13}$$

$$C_3H_7OH + CO + 2H_2 \rightarrow C_4H_9OH + H_2O \tag{14}$$

Furthermore, CO_2 is formed via the water-gas shift reaction:

$$CO + H_2O \; CO_2 + H_2 \tag{15}$$

In kinetic modelling all other reactions are assumed to be irreversible apart from the water gas shift reaction. A powder-law kinetic model was proposed for syngas transformation to higher alcohols including the following reaction rates[42] for individual components taking into account the influence of the alcohol formed in the previous step, e.g. methanol in the rate equation of ethanol formation. Overall, the rate equations can be written as follows:

$$r_{CH3OH} = k_{CH3OH} p_{CO}^{a} P_{H2}^{b} \tag{16}$$

$$r_{CH4} = k_{CH4} p_{CH3OH}^{c} p_{H2}^{d} \tag{17}$$

$$r_{C2H5OH} = k_{C2H5OH} p_{CH3OH} p_{CO}^{e} p_{H2}^{f} \tag{18}$$

$$r_{C3H7OH} = k_{C3H7OH} p_{C2H5OH}^{h} p_{CO}^{i} p_{H2}^{j} \tag{19}$$

$$r_{C4H9OH} = k_{C4H9OH} p^{k}_{C3H7OH} p^{l}_{CO} p^{m}_{H2} \quad (20)$$

$$r_{CO2} = kP_{CO} - \left(\frac{k}{K_{WGS}}\right) P_{CO2} \quad (21)$$

Reactor modelling for an ideal plug-flow reactor includes mole balances for each compound:

$$\frac{dF_{CO}}{dW} = -(r_{CH3OH} + r_{C2H5OH} + r_{C3H7OH} + r_{CO2}) \quad (22)$$

$$\frac{dF_{H2}}{dW} = -(2r_{CH3OH} + 2r_{C2H5OH} + 2r_{C3H7OH} + r_{CH4}) + r_{CO2} \quad (23)$$

$$\frac{dF_{H2O}}{dW} = r_{C2H5OH} + r_{C3H7OH} + r_{CH4} - r_{CO2} \quad (24)$$

$$\frac{dF_{CH3OH}}{dW} = r_{CH3OH} - r_{C2H5OH} - r_{CH4} \quad (25)$$

$$\frac{dF_{C2H5OH}}{dW} = r_{C2H5OH} - r_{C3H7OH} \quad (26)$$

$$\frac{dF_{C3H7OH}}{dW} = r_{C3H7OH} \quad (27)$$

$$\frac{dF_{C4H9OH}}{dW} = -r_{C3H7OH} \quad (28)$$

$$\frac{dF_{CH4}}{dW} = r_{CH4} \quad (29)$$

$$\frac{dF_{CO2}}{dW} = r_{CO2} \quad (30)$$

in which F_i denotes the molar flow of a component i and W is the catalyst mass. The values of the reaction orders and activation energies were determined by the data fitting.[42] Analogous considerations were applied in,[25] however, taking into account also pentanol formation. Reaction orders reported in different studies are shown in Table 3. Reaction orders have been calculated for formation of different species, e.g. methane, C_2H_n, C_3H_n, methanol and ethanol with respect to H_2 and CO, respectively.[30] The species C_2H_n and C_3H_n denote hydrocarbons with either carbon number 2 or 3, respectively. The results revealed that negative or close to zero order was found for CO in methane and methanol formation, while especially at 280 °C a close to zero order dependence with respect to CO was observed for formation of C_3H_n over $CoCu/SiO_2$ catalyst. The Langmuir-Hinshelwood model with dissociative adsorption of H_2 and CO was applied reasoning that a negative reaction order in CO indicates strong adsorption of CO or formation of carbon containing the surface species which may retard adsorption and dissociation of H_2.

A more simple power law model was applied in[30] considering that alcohols are formed directly from syngas:

$$r_i = k p^{m}_{CO} p^{n}_{H2} \quad (31)$$

One-dimensional quasi-homogeneous plug flow reactor model was used to described the influence of reactants, alkanes, alcohols, alkenes as well as CO_2.[32] The deviations were minimized in the objective function using the Levenberg-Marquardt algorithm. In[73] methanol formation was regarded as a reversible equilibrium reaction:

$$r_{CH3OH} = k_{CH3OH}\left(p^{a}_{CO} p^{b}_{H2} - p^{c}_{CH3OH}/K_{CH3OH}\right) \quad (32)$$

Ethanol was considered to be formed only from 2 moles of methanol without involvement of CO and H_2 pressure in the kinetic expressions:

$$r_{C2H5OH} = k_{C2H5OH} p^{a}_{CH3OH} \quad (33)$$

Correspondingly kinetics of propanol formation was described using the partial pressures of methanol and ethanol as follows:

$$r_{C3H7OH} = k_{HA} p^{a}_{CH3OH} p^{b}_{C2H5OH} \quad (34)$$

This approach does not have a clear mechanistic interpretation.

Table 3. Reaction orders with respect to H_2 and CO in syngas transformation to higher alcohols.

Product	Catalyst											
	K–$CoMoS_2$[42]			K–CoRhMo supported on carbon nanohorn[25]			Co–Rh–Mo–K/MWCNT[72]		CuCo[32]		$CoCu/SiO_2$[70]	
	H_2	CO	$C_{n\text{-}1\text{-}OH}$	H_2	CO	$C_{n\text{-}1}OH$	H_2	CO	H_2	CO	H_2	CO
Methane	0.6	n.a.	n.a.	1	1	n.a.	n.a.	n.a.	1.07	−0.52	0.97	−0.83
Ethene	n.a.	n.a.	n.a.	>0	>0	n.a.	n.a.	n.a.	0.17	1.1	0.69	−0.43
Ethane	n.a.	n.a.	n.a.	>1	>1	n.a.	n.a.	n.a.	1.31	−0.62	n.a.	n.a.
Propane	n.a.	n.a.	n.a.	0.5	0.5	n.a.	n.a.	n.a.	0.6	0.05	0.81[d]	−0.28
MeOH	0.44	1.85		1.2	1.2		1.89[a]	0.87[b] 0.765[c]	1.25	−0.32	1.63	0.07
EtOH	1.39	0.75	0.24	1	1	1.0	n.a.	n.a.	1.02	0	1.05	0.09
C3OH	0.28	1.0	1.22	1.28	1.31	0.78	n.a.	n.a.	0.7	0.22	n.a.	n.a.
C4OH	n.a.	n.a.	0.59	1.0	0.28	1.0	n.a.	n.a.	0.52	0.52	n.a.	n.a.
C5OH	n.a.	n.a.	n.a.	1.0	1.0	1.0	n.a.	n.a.	0.52	0.71	n.a.	n.a.
CO_2	n.a.	n.a.	n.a.	1.0	1.0	n.a.	n.a.	n.a.	n.a.	n.a.	n.a.	n.a.

[a, b, c] constants in eq. (32), [d] for C_3H_n denote hydrocarbons with three carbon atoms.

Activation energies for formation of different products reported in Table 4 suggest that hydrogenation is more prominent at higher temperatures and at the same time the chain length probability decreases[32] Olefin formation is inhibited at higher temperatures, while CO_2 formation is promoted by the water-gas shift reaction.[41,52] When comparing the activation energies for formation of methane and methanol or ethane and ethanol, it can be seen that these values for alcohol formation are lower than for hydrocarbons, when using sulfided K–CoRhMo supported on carbon nanohorn (CNH) catalyst (Table 4). Analogously in[42] the activation energies for methanol and ethanol determined with a power model were much lower than for C3–C4 alcohols over K–$CoMoS_x$ catalyst. The activation energy for methane formation was rather high (Table 4) indicating that this catalyst could be thus more effective towards formation of higher alcohols. Overall, it can be concluded that higher alcohol formation is promoted at lower temperatures. Furthermore, the activation energies for formation of different alcohols decreased with increasing the chain length of the alcohol,[25] although in[42] the activation energy for ethanol was lower than for methanol.

5. Scale-up and Methods to Enhance Higher Alcohol Formation

Some efforts to scale up higher alcohol production have been made by industrial engineering and manufacturing companies (SEHT, Lurgi and Sűd Chemie, Snamprogetti, Dow Chemicals and Union Carbide, Institut Francais du Pétrole) at different levels using K-ZnCr (Cu) (industrial plant), K–CuZnAl (pilot), K–MoS_2, K–$CNiMoS_2$, K–CuCoAl and K–CuNiTi (pilot) based catalysts.[71] The former catalyst required high temperatures and pressures of 330–430 °C and 9–18 MPa, respectively, while the latter ones were used at 250–350 °C and 5–20 MPa, respectively. Typically, the H_2/CO ratio in these processes was in the range of 0.5–1.8. The highest fraction of C3–C5 alcohols over alkali modified Cu/Zn/Cr catalyst was 31%, while the fraction of methanol and ethanol was 69%.[71]

Apparently, a high carbon efficiency in terms of higher alcohols is required for a feasible industrial operation, therefore several methods, such as recycling of light alcohols[69,73,74] and addition of non-reactive solvents to facilitate a good temperature control,[72] have been proposed to increase the yields of higher alcohols. Recycling of light alcohols was tested in,[73] where methanol, ethanol and propanol were separated and send back to the reactor with the syngas.[73] It was reported that the amount of butanol increased to 54.4 wt% in the liquid products, when the syngas was fed together with 7.5% of mixed light alcohols into the reactor in syngas transformation using a catalyst at 320–350 °C under 103 bar and H_2/CO ratio of 1 and 3000 l/kg/h liquid hourly space velocity and small amounts of a solvent. Unfortunately, more details were not provided in the patent. Another method was to use a preconverter to produce methanol from syngas and a multibed quench reactor for production of higher alcohols. Methanol formed in the preconverter, was fed together with syngas to another reactor. The light alcohols and the gas phase were separated from higher alcohols and fed back to the second reactor. It was reported that in the final process design comprising liquid and gas phases recycling it was possible to obtain 99.9% of higher alcohols, mainly isobutanol and higher alcohols.[73]

Furthermore, co-feeding of methanol in syngas transformation to higher alcohols was investigated in[75] using K-MoS_2 catalyst showing that with increasing amounts of the co-fed methanol, formation of higher alcohols was elevated. It was additionally suggested that a techno-economic analysis should be made to optimize the amount of methanol to be recycled.

6. Conclusions and Future Prospects

Higher alcohol synthesis from syngas is an important reaction currently being intensively investigated because syngas can be obtained via gasification of biomass and also there is a rapidly growing interest in waste to syngas technologies. Besides utilization of higher alcohols in production of plastics, or as fuel additives, one emerging use for higher alcohols formed from biomass is their utilization for synthesis of sustainable aviation fuel, as they are not competing with the food supply chain. The main challenge in higher alcohol synthesis from syngas is rather low selectivity and space time yield of the desired products.

Table 4. Activation energies (kJ/mol) for formation of different hydrocarbons and alcohols. Notation: MWCNT multiwalled carbon nanotube, CNF carbon nanofiber, HC = unsaturated hydrocarbon.

Product	K–CuFe/CNF[41]	CuCo[32]	K–$CoMoS_2$[42]	K–CoRhMo supported on carbon nanohorn[25]	CoRhMo/MWCNT[72]	CoCu/SiO_2[30]
Methane	143	172	126	126.4		125
Ethene	85[a]	73	n.d.	n.d.	n.d.	n.d.
Ethane	106[b]	196	n.d.	n.d.	112	123
Propane	n.a.	149	n.d.	n.d.	n.d.	118
MeOH	117	122	63	36.1	35	54
EtOH	142[c]	129	54	54.4	57	79
C3OH	n.d.	121	82	92.2	94[c]	n.d.
C4OH	n.d.	n.d.	104	148.6	n.d.	n.d.
C5OH	n.d.	n.d.	n.d.	126.4	n.d.	n.d.
CO_2	n.d.	n.d.	146	90.7	n.d.	n.d.

[a] higher unsaturated hydrocarbons, [b] higher saturated hydrocarbons, [c] for higher alcohols.

The highest space time yield of alcohols have been obtained with bimetallic potassium modified copper-iron catalyst supported on a hierarchical zeolite. The desired catalysts exhibit relatively small metal particles, which facilitate higher alcohol formation and limit generation of CO_2. Alloys have also a beneficial effect on higher alcohol formation, providing a close contact between the two metals with separate functions, e.g. copper for hydrogenation and iron for the chain growth. Among efficient catalysts sodium modified cobalt-iron catalyst was reported. The role of alkali metal promoters is to ensure a high metal dispersion of the active metal and coexistence of the metal oxide phase after reduction. The active sites during synthesis of higher alcohols from syngas are cobalt or iron carbides, which are created upon syngas exposure to the reduced catalyst. Recently several advanced tools, such as DRIFTs-MS have been used to identify reaction intermediates and facilitate development of even more selective catalysts.

The desired reaction conditions typically are a rather low temperature of 225–300 °C under relatively high pressures, and the H_2/CO ratio of 1–2. On the other hand, too high pressure can also decrease selectivity to the alcohols due to enhanced dehydration.

From the mechanistic point of view a dual site model has been commonly accepted, in which two different sites promote associative and dissociative CO adsorption. The latter is needed for the chain growth while associative adsorption of CO facilitates alcohol formation. In addition to addressing the desired catalyst properties and reaction conditions, thermodynamic data, kinetic analysis and modelling, as well as scale-up issues were also summarized. According to thermodynamics formation of C4 alcohols is thermodynamically favored at lower temperatures, e.g. at 277 °C, while the undesired water gas shift reaction is promoted at higher temperatures. The product distribution is apparently sensitive to the thermodynamic model used, as in some studies 2-propanol was calculated as the most prominent product at higher temperatures.

In addition to addressing the desired catalyst properties and reaction conditions, thermodynamic data, kinetic analysis and modelling, as well as scale-up issues were also summarized. According to thermodynamics, formation of C4 alcohols is thermodynamically favored at lower temperatures, e.g. at 277 °C, while the undesired water gas shift reaction is promoted at higher temperatures. The product distribution is apparently sensitive to the thermodynamic model used, as in some studies 2-propanol was calculated as the most prominent product at higher temperatures.

Based on the experimental results the syngas gas transformations gave the highest alcohol selectivity at intermediate temperatures and pressures, such as 250 °C and 5 MPa, respectively over potassium modified copper-iron catalyst supported on carbon nanofibers. Slightly higher temperatures were required for molybdenum based catalysts.

In kinetic modelling mainly power law models have been applied. Typically, the reaction order with respect to hydrogen for formation of alcohols and hydrocarbons is close to one being positive, while negative or close to zero order has been obtained for CO. Activation energies for formation of lower alcohols have been typically smaller than those for higher alcohols also indicating that higher alcohol formation is promoted at lower temperatures.

Some scale-up concepts including recirculation of lower alcohols and installing a preconverter for methanol have been investigated. From the industrial point of view, it has been suggested that these types of concepts require additional feasibility justification involving e.g. a detailed techno-economic analysis.

Acknowledgements

The authors are grateful to Business Finland for funding the SynJet project.

Conflict of Interest

The authors declare no conflict of interest.

Data Availability Statement

The data that support the findings of this study are available from the corresponding author upon reasonable request.

Keywords: heterogeneous catalyst · higher alcohol · syngas

[1] H. T. Luk, C. Mondelli, D. C. Ferré, J. A. Stewart, J. Pérez-Ramírez, *Chem. Soc. Rev.* **2017**, *46*(5), 1358–1426.
[2] Z. Li, Z. Zeng, D. Yao, S. Fan, S. Guo, J. Lv, S. Huang, Y. Wang, X. Ma, *ACS Sustainable Chem. Eng.* **2020**, *8*, 200–209.
[3] Fatty Alcohol Market Size, Share & Trends Analysis By Product (C6–C10, C11–C14, C15–C22), By Application (Soaps & Detergents, Personal Care, Lubricants, Amines), By Region, And Segment Forecasts, 2015–2022, https://www.grandviewresearch.com/industry-analysis/fatty-alcohols-market, accessed 5.8.2022.
[4] V. V. Maximov, E. A. Permyakov, V. S. Dorokhov, A. Wang, P. J. Kooyman, V. M. Kogan, *ChemCatChem* **2020**, *12*(5), 1443–1452.
[5] F. Zeng, X. Xi, H. Cao, Y. Pei, H. J. Heeres, R. Palkovits, *Appl. Catal. B* **2019**, *246*, 232–241.
[6] E. T. Liakakou, M. A. Isaacs, K. Wilson, A. F. Lee, E. Heracleous, *Catal. Sci. Technol.* **2017**, *7*(4), 988–999.
[7] M. Braun-Unkhoff, U. Riedel, *CEAS Aeronautical J.* **2015**, *6*(1), 83–93.
[8] E. Yoo, U. Lee, M. Wang, *ACS Sustainable Chem. Eng.* **2022**, *10*(27), 8725–8732.
[9] I. Abrantes, A. F. Ferreira, A. Silva, M. Costa, *J. Cleaner Prod.* **2021**, *313*, 127937.
[10] M. A. Díaz-Pérez, J. C. Serrano-Ruiz, *Molecules* **2020**, *25*(4), 802.
[11] H. Wei, W. Liu, X. Chen, Q. Yang, J. Li, H. Chen, *Fuel* **2019**, *254*, 115599.
[12] S. Geleynse, K. Brandt, M. Garcia-Perez, M. Wolcott, X. Zhang, *ChemSusChem* **2018**, *11*(21), 3689–3689.
[13] D. J. Gregg, J. N. Saddler, *Biotechnol. Bioeng.* **1996**, *1*(4), 375–383.
[14] M. L. Rabinovich, *Cell. Chem. Technol.* **2010**, *44* (4–6) 173–186.
[15] T. Riittonen, K. Eränen, A. Schchukarev, P. Mäki-Arvela, A.-R. Rautio, K. Kordas, N. Kumar, T. Salmi, J.-P. Mikkola, *J. Renew. Energy* **2015**, *74*, 369–378.
[16] F. Cheng, C. E. Brewer, *Renewable Sustainable Energy Rev.* **2017**, *72*, 673–722.
[17] L. Yang, Z. Song, Y. Yu, L. Zhu, D. Xia, *Catal. Surv. Asia* **2020**, *24*(2), 104–114.
[18] Z. Y. Du, B. B. Zhang, T. S. Chen, Y. Betancur, W. Y. Li, *Energy Fuels* **2019**, *33*(10), 10176–10184.

[19] M. J. Cordon, J. Zhang, S. C. Purdy, E. C. Wegener, K. A. Unocic, L. F. Allard, M. Zhou, R. S. Assary, J. T. Miller, T. R. Krause, F. Lin, H. Wang, A. J. Kropf, C. Yang, D. Liu, Z. Li, *ACS Catal.* **2021**, *11*(12), 7193–7209.
[20] V. L. Dagle, A. D. Winkelman, N. R. Jaegers, J. Saavedra-Lopez, J. Hu, M. H. Engelhard, S. E. Habas, S. A. Akhade, L. Kovarik, V.-A. Glezakou, R. Rousseau, Y. Wang, R. A. Dagle, *ACS Catal.* **2020**, *10*(18), 10602–10613.
[21] M. A. Lilga, R. T. Hallen, K. O. Albrecht, A. R. A. R. Cooper, J. G. Frye, K. K. Ramasamy, US 10,005,974, **2018**.
[22] Plasco Energy group, Solid waste to syngas-from demonstration to commercialization, https://www.altenergymag.com/article/2013/02/solid-waste-to-syngasfrom-demonstration-to-commercialization/1197, date of access 23.9.2022.
[23] W. Aslam, J. N. Beltramini, L. A. Atanda, N. R. Batalha, T. U. Schülli, M. Konarova, *Appl. Catal. A* **2020**, *605*, 117803.
[24] W. Aslam, H. M. Ahmed, T. Qui, M. Konarova, *Chem. Eng. J. Adv.* **2020**, *3*, 100024.
[25] P. E. Boahene, A. K. Dalai, *Ind. Eng. Chem. Res.* **2018**, *57*(16), 5517–5528.
[26] P. E. Boahene, R. Sammynaiken, A. K. Dalai, *Int. J. Petrochem. Sci. Eng.* **2017**, *2*(1), 00023.
[27] T.-Y. Chen, J. Su, Z. Zhang, C. Cao, X. Wang, R. Si, X. Liu, B. Shi, J. Xu, Y.-F. Han, *ACS Catal.* **2018**, *8*, 8606–8617.
[28] W. G. Cui, Y. T. Li, H. Zhang, Z. C. Wei, B. H. Gao, J. J. Dai, T. L. Hu, *Appl. Catal. B* **2020**, *278*, 119262.
[29] S. Fan, Y. Wang, Z. Li, Z. Zeng, D. Yao, S. Huang, X. Ma, *Appl. Catal. A* **2019**, *583*, 117123.
[30] J. Su, W. Mao, X. C. Xu, Z. Yang, H. Li, J. Xu, Y. F. Han, *AIChE J.* **2014**, *60*(5), 1797–1809.
[31] E. A. Gorlov, A. V. Shumovskii, Y. P. Yas'yan, M. Y. Niskovskaya, M. S. Kotelev, E. M. Smirnova, A. A. Ol'gin, *Petrol. Chem.* **2019**, *59*(11), 1249–1255.
[32] C. Göbel, S. Schmidt, C. Froese, T. Bujara, V. Scherer, M. Muhler, *J. Catal.* **2021**, *394*, 465–475.
[33] C. Göbel, S. Schmidt, C. Froese, Q. Fu, Y. T. Chen, Q. Pan, M. Muhler, *J. Catal.* **2020**, *383*, 33–41.
[34] C. Huang, C. Zhu, M. Zhang, J. Chen, K. Fang, *Appl. Catal. B* **2022**, *300*, 120739.
[35] F. Li, J. Li, K. Wang, M. Ao, J. Qiu, X. Zhang, H. Wang, G. H. Pham, S. Liu, *Compos. Part B-Eng.* **2021**, *209*, 108608.
[36] Y. Li, W. Gao, M. Peng, J. Zhang, J. Sun, Y. Xu, S. Hong, X. Liu, X. Liu, M. Wei, B. Zhang, D. Ma, *I. Nat. Commun.* **2020**, *11*, 61.
[37] F. Li, Q. Zhang, J. Liu, N. Cui, G. Guan, W. Huang, *Green Energy & Environ.* **2022**, https://doi.org/10.1016/j.gee.2022.01.015.
[38] T. Lin, X. Qi, X. Wang, L. Xia, C. Wang, F. Yu, H. Wang, S. Li, L. Zhong, Y. Sun, *Angew. Chem. Int. Ed.* **2019**, *58*, 4627–4631; *Angew. Chem.* **2019**, *131*, 4675–4679.
[39] B. Liu, Y. Li, Y. Duan, T. Ding, Y. Tang, C. Zheng, *React. Kinet. Mech. Catal.* **2019**, *128*, 695–706.
[40] H. T. Luk, C. Mondelli, S. Mitchell, D. C. Ferré, J. A. Stewart, J. Pérez–Ramírez, *J. Catal.* **2019**, *371*, 116–125.
[41] H. T. Luk, C. Mondelli, S. Mitchell, S. Siol, J. A. Stewart, D. Curulla Ferré, J. Pérez-Ramírez, *ACS Catal.* **2018**, *8* (10), 9604–9618.
[42] L. Negahdar, X. Xi, F. Zeng, J. G. M. Winkelman, H. J. Heeres, R. Palkovits, *Int. J. Chem. Kinet.* **2021**, *53*(3), 419–427.
[43] J. Paterson, M. Peacock, R. Purves, R. Partington, K. Sullivan, G. Sunley, J. Wilson, *ChemCatChem* **2018**, *10*(22), 5055–5055.
[44] T. Qin, T. Lin, X. Qi, C. Wang, L. Li, Z. Tang, L. Zhong, Y. Sun, *Appl. Catal. B* **2021**, *285*, 119840.
[45] M. Shui, C. Huang, P. Ma, W. Li, Q. He, W. Wu, Y. Tan, J. Bao, *Chin. Chem. Lett.* **2021**, *32*(7), 2203–2206.
[46] K. Sun, M. Tan, Y. Bai, X. Gao, P. Wang, N. Gong, T. Zhang, G. Yang, Y. Tan, *J. Catal.* **2019**, *378*, 1–16.
[47] I. C. ten Have, E. Valle, A. Gallo, J. L. Snider, M. S. Duyar, T. F. Jaramillo, *Energy Technol.* **2019**, *7*(5), 1801102.
[48] C. Wang, H. Yu, T. Lin, X. Qi, F. Yu, L. Zhong, Y. Sun, *Catal. Sci. Technol.* **2022**, *12*(5), 1697–1708.
[49] C. Wang, T. Lin, X. Qi, F. Yu, Y. Lu, L. Zhong, Y. Sun, *J. Phys. Chem. C* **2021**, *125*(11), 6137–6146.
[50] W. Yang, M. Chen, J. Zhou, Y. Duan, Y. An, M. Liu, M. Tian, *Appl. Catal. A* **2020**, *608*, 117868.
[51] Y. Xu, H. Ma, H. Zhang, W. Qian, Q. Sun, W. Ying, D. Chen, *Catalysts* **2020**, *10*(10).
[52] Z. Zeng, Z. Li, T. Guan, S. Guo, Z. Hu, J. Wang, A. Rykov, J. Lv, S. Huang, Y. Wang, X. Ma, *J. Catal.* **2022**, *405*, 430–444.
[53] Z. Zeng, Z. Li, S. Guo, J. Lv, S. Huang, Y. Wang, X. Ma, *ACS Sustainable Chem. Eng.* **2021**, *9*(33), 11258–11268.
[54] J. Zhang, Y. Li, *Kinet. Catal.* **2020**, *61*(6), 861–868.
[55] L. Zhao, J. Duan, Q. Zhang, Y. Li, K. Fang, *Ind. Eng. Chem. Res.* **2018**, *57*, 14957–14966.
[56] L. Zhao, Y. Li, X. Liu, K. Fang, *Catal. Today* **2020**, *355*, 17–25.
[57] Z. Zhao, W. Lu, R. Yang, H. Zhu, W. Dong, F. Sun, Z. Jiang, Y. Lyu, T. Liu, H. Du, Y. Ding, *ACS Catal.* **2018**, *8*, 228–241.
[58] M. Ao, G. H. Pham, J. Sunarso, M. O. Tade, S. Liu, *ACS Catal.* **2018**, 8, 7025–7050.
[59] T. Lin, F. Yu, Y. An, T. Qin, L. Li, K. Gong, L. Zhong, Y. Sun, *Accounts of Chem. Res.* **2021**, *54*(8), 1961–1971.
[60] Y. Yang, L. Wang, K. Xiao, T. Zhao, H. Wang, L. Zhong, Y. E. Sun, *Catal. Sci. Technol.* **2015**, *5*(8), 4224–4232.
[61] J. G. Nunan, C. E. Bogdan, K. Klier, K. J. Smith, C. W. Young, R. G. Herman, *J. Catal.* **1988**, *113*(2), 410–433.
[62] H. Er-Rbib, C. Bouallou, *Energy* **2014**, *75*, 81–88.
[63] R. P. Ye, J. Ding, W. Gong, M. D. Argyle, Q. Zhong, Y. Wang, C. K. Russell, Z. Xu, A. G. Russell, Q. Li, M. Fan, Y.-G. Yao, *Nat. Commun.* **2019**, *10*(1), 1–15.
[64] T. Toyoda, T. Minami, E. W. Qian, *Energy Fuels* **2013**, *27*(7), 3769–3777.
[65] C. Huang, C. Zhu, M. Zhang, Y. Lu, Q. Wang, H. Qian, J. Chen, K. Fang, *ChemCatChem* **2021**, *13*(13), 3184–3197.
[66] F. Kleitz, S. H. Choi, R. Ryoo, *Chem. Commun.* **2003**, *17*, 2136–2137.
[67] W. Hummers, R. E. Offeman, *J. Am. Chem. Soc.* **1958**, *80*(6), 1339–1339.
[68] E. Tronconi, P. Forzatti, I. Pasquon, *J. Catal.* **1990**, *124*(2), 376–390.
[69] S. Mawson, M. S. McCutchen, P. K. Lim, G. W. Roberts, *Energy Fuels* **1993**, *7*(2), 257–267.
[70] M. Grzesik, M. Kulawska, J. Skrzypek, M. Witczak, *Stud. Surf. Sci. Catal.* **1999**, *122*, 411–414.
[71] R. Andersson, in *Catalytic conversion of syngas to higher alcohols over MoS2-based catalysts*, doctoral dissertation, KTH Royal Institute of Technology, Stockholm, Sweden, **2015**.
[72] V. R. Surisetty, A. K. Dalai, J. Kozinski, *Energy Fuels* **2010**, *24*(8), 4130–4137.
[73] P. J. Tijm, F. Baksh, US patent 8921431 B2, 2014.Method for improving higher alcohol yields from syngas by altering flow regimes within a reactor.
[74] H. Modarresi, C. Wix, US patent 2015/0315109 A1. Process and apparatus for the production of higher alcohols.
[75] M. P. Crespo, A. V. Perales, F. Vidal-Barrero, M. Campoy, *Fuel Process. Technol.* **2015**, *134*, 270–274.

Manuscript received: August 9, 2022
Revised manuscript received: September 27, 2022
Accepted manuscript online: September 28, 2022
Version of record online: ■■, ■■■

REVIEW

Recent developments in transformations of syngas to higher alcohols are critically summarized. Especially there is an urgent need to develop jet fuels form sustainable sources, and higher alcohols are a potential source. The highest space time yields of higher alcohols of 0.61 g/(g_{cat}h) is obtained over a bimetallic copper-iron catalyst supported on a hierarchical zeolite at 300 °C and 5 MPa. Other potential catalysts that are promising for the direct synthesis of higher alcohols from syngas are copper-cobalt and cobalt-manganese compositions The main challenge in transformation of syngas to higher alcohols is to suppress formation of alkanes and CO_2. A dual site catalyst is required, facilitating both hydrogenation and chain growth. In addition to finding optimum reaction conditions and catalyst properties based on literature, kinetic modelling, thermodynamics and scale up issues are discussed.

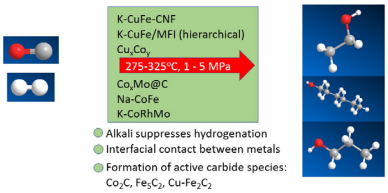

*Prof. P. Mäki-Arvela, Dr. A. Aho, Dr. I. Simakova, Prof. D. Yu. Murzin**